Monthly Notices
of the
ROYAL ASTRONOMICAL SOCIETY

MNRAS **467,** 873–897 (2017)
Advance Access publication 2017 January 12

doi:10.1093/mnras/stx068

The intrinsic and interstellar broad-band linear polarization of nearby FGK dwarfs

Daniel V. Cotton,[1,2]★ Jonathan P. Marshall,[1,2,3] Jeremy Bailey,[1,2] Lucyna Kedziora-Chudczer,[1,2] Kimberly Bott,[1,2,4,5] Stephen C. Marsden[3] and Bradley D. Carter[3]

[1]*School of Physics, UNSW Australia, NSW 2052, Australia*
[2]*Australian Centre for Astrobiology, UNSW Australia, NSW 2052, Australia*
[3]*Computational Engineering and Science Research Centre, University of Southern Queensland, Toowoomba, Qld. 4350, Australia*
[4]*University of Washington Astronomy Department, Box 351580, UW Seattle, WA 98195, USA*
[5]*NASA Astrobiology Institute Virtual Planetary Laboratory, Box 351580, UW Seattle, WA 98195, USA*

Accepted 2017 January 10. Received 2016 December 15; in original form 2016 September 15

ABSTRACT

We present linear polarization measurements of nearby FGK dwarfs to parts-per-million (ppm) precision. Before making any allowance for interstellar polarization, we found that the active stars within the sample have a mean polarization of 28.5 ± 2.2 ppm, while the inactive stars have a mean of 9.6 ± 1.5 ppm. Amongst inactive stars, we initially found no difference between debris disc host stars (9.1 ± 2.5 ppm) and the other FGK dwarfs (9.9 ± 1.9 ppm). We develop a model for the magnitude and direction of interstellar polarization for nearby stars. When we correct the observations for the estimated interstellar polarization, we obtain 23.0 ± 2.2 ppm for the active stars, 7.8 ± 2.9 ppm for the inactive debris disc host stars and 2.9 ± 1.9 ppm for the other inactive stars. The data indicate that whilst some debris disc host stars are intrinsically polarized most inactive FGK dwarfs have negligible intrinsic polarization, but that active dwarfs have intrinsic polarization at levels ranging up to ∼45 ppm. We briefly consider a number of mechanisms, and suggest that differential saturation of spectral lines in the presence of magnetic fields is best able to explain the polarization seen in active dwarfs. The results have implications for current attempts to detect polarized reflected light from hot Jupiters by looking at the combined light of the star and planet.

Key words: techniques: polarimetric – stars: activity – circumstellar matter – stars: solar-type – dust, extinction – ISM: magnetic fields.

1 INTRODUCTION

Scattering from cloud particles in planetary atmospheres polarizes light. A number of efforts have been made (Berdyugina et al. 2008, 2011; Lucas et al. 2009; Wiktorowicz 2009) and are underway (Wiktorowicz et al. 2015; Bott et al. 2016) to detect reflected light from hot Jupiter atmospheres in the combined light of the star and planet using broad-band aperture polarimetry. A signal should show up as a variable polarization around the orbital cycle, with a peak near ∼20 ppm in blue light expected in the most promising systems (Seager, Whitney & Sasselov 2000; Bott et al. 2016). In such work, it is usually assumed that the light from the star is unpolarized but there is very little evidence to support such an assertion at the needed precision.

High-precision polarimetric surveys of nearby stars have been conducted by Bailey, Lucas & Hough (2010) in a red (575–1025 nm) bandpass, and Cotton et al. (2016a,b) in the Sloan Digital Sky Survey (SDSS) g' band (green) – which is more relevant to exoplanet work. These surveys identified intrinsic polarization from extreme stellar types (late giants, B- and Be-stars, Ap stars) and some debris disc systems, but none from ordinary main-sequence stars. However, both of these surveys were magnitude-limited, and as a result, included very few later type main-sequence stars. The aim of this study is to extend that work further down the main sequence.

Parts-per-million (ppm) polarimetry of the fainter main-sequence stars has only recently become possible (Hough et al. 2006; Kochukhov et al. 2011), and to date, there are no convincing determinations of the level of broad-band polarization in FGK dwarfs. Kemp et al. (1987b) used a special instrumental arrangement to measure the whole disc of the quiet Sun, obtaining a linear polarization of <0.3 ppm. Yet, there is some reason to suspect that broad-band

★ E-mail: d.cotton@unsw.edu.au

polarization may manifest in FGK dwarfs. The (transverse component of) magnetic fields associated with starspot regions on the Sun produce linear polarization in spectral lines as a result of the Zeeman Effect (Donati & Landstreet 2009). Where there are sufficient spectral lines blanketing a band, the combined effect may be enough to produce a measurable linear polarization; the mechanism is properly known as *differential saturation*[1] after the differential saturation of the π and σ components of the Zeeman multiplet that occurs in the transfer of radiation in a stellar atmosphere (Bagnulo et al. 1995). Early on, Tinbergen & Zwaan (1981) invoked this mechanism in what they described as an 'attractive hypothesis' to explain a weak trend to higher polarizations with later spectral type in stars from F0 onwards. The idea was developed by many including Landi Degl'Innocenti (1982), Leroy (1990), Huovelin & Saar (1991), Saar & Huovelin (1993) and Stift (1997), who made calculations based on fields localized in starspots. In contrast to those predictions, more recent spectropolarimetric measurements of circular polarization have revealed large-scale magnetic fields of varying complexity, that appear not to be associated with cool spots (Donati & Landstreet 2009; Fares et al. 2010; Morgenthaler et al. 2012; Jeffers et al. 2014). Linear polarization has been detected in the spectral lines of active cool stars (Kochukhov et al. 2011; Rosén, Kochukhov & Wade 2013, 2015), which can, in principle, be used to derive the broad-band linear polarization (Wade et al. 2000). Yet, to date, there are no satisfying systematic measurements of the effect of such magnetic fields in linear broad-band polarization. Huovelin, Saar & Tuominen (1988) made measurements that attempted to correlate broad-band linear polarization with the activity indicator $\log(R'_{HK})$. However, the sensitivity of their instrument meant they had to rely on statistical techniques that only considered measurements 2σ from the mean. According to Clarke (1991), these observations were contested at the time by Leroy (1989) and others as being unreliable due to problems with scattered moonlight (particularly in U band), and he would later describe this area of research as 'abandoned' (Clarke 2010). Yet, Alekseev (2003) and most recently, Patel et al. (2016) have copied the multiband approach of Huovelin et al. (1988), with similar results – finding increased levels of polarization in shorter wavelength bands for active dwarfs, which Patel et al. (2016) assign to a combination of differential saturation and scattering processes.

Aside from possibly differential saturation, in FGK dwarfs, measurable polarization will be present in some debris disc systems, such as those observed by Hough et al. (2006), Bailey et al. (2010) and Wiktorowicz & Matthews (2008), due to scattering from the dust grains in the discs. The magnitude and direction of the polarization is a function of the disc geometry with respect to the aperture and line of sight, and the size, shape, composition and porosity of the dust grains. Clarke (2010)'s comprehensive text book relates no other detections or prospects for detection in solar type stars. The sole exception being the young (∼70 Myr) star HD 129333 studied by Elias & Dorren (1990), which exhibited an unexplained polarization angle variation unconnected to its rotational period. In this case, the authors suggested that the most likely cause of the polarization was scattering from a circumstellar envelope modulated by the motion of an unseen companion.

[1] Many of the authors we cite on this topic refer to the phenomenon as magnetic intensification rather than differential saturation. However magnetic intensification (Babcock 1949) does not necessarily involve the line-blanketing necessary to generate broad-band linear polarization, and so we prefer differential saturation here.

In contrast to the *intrinsic polarization* related to the stars themselves (or their immediate surrounds), the light reaching us from all stars is extrinsically polarized by aligned dust grains in the interstellar medium (ISM). This *interstellar polarization* is largely constant for any given star system, but acts to confound measurements of intrinsic polarization. In distant stars, the sheer magnitude of interstellar polarization can swamp any intrinsic signal. In nearby space, the region known as the Local Hot Bubble (LHB), extending out to ∼75 to 150 pc from the Sun, is largely devoid of dust and gas. In this region, the ISM is polarized at a rate of ∼0.2–2 ppm pc^{-1} (Cotton et al. 2016a). This is small, at least an order of magnitude smaller than the region beyond the LHB (Behr 1959), but when seeking intrinsic effects at the level of tens of parts-per-million, it is significant and needs to be subtracted. Frisch et al. (2016) are working on improving their mapping of the ISM field in nearby space. Broad-band stellar optical polarimetry will help in this task (Frisch et al. 2012), but at present, the data within 50 pc are sparse (especially at southern latitudes). As a result, the local interstellar polarization tends to be neglected, as it has been in the studies of active late dwarfs mentioned above.

In the following sections of this paper, we describe a polarimetric survey of FGK dwarfs. We begin with details of the observations (Section 2) and the results of those observations (Section 3). We then make an initial analysis of the results to attempt to identify statistical differences between active stars and inactive stars, and between debris disc host stars and ordinary FGK dwarfs (Section 4.1). After that, we add the appropriate parts of our data set to measurements from the literature in order to develop a model to describe interstellar polarization in the nearby ISM (Section 4.2); some comments are made about the nature of the ISM in passing. In Section 4.3, we carry out a vector subtraction using our simple model to calculate the intrinsic polarization of the programme stars. Following this, we examine and discuss the intrinsic polarization in ordinary FGK dwarfs (Section 4.4), debris disc host systems (Section 4.5) and active stars (Section 4.6). Our conclusions are presented in Section 5.

2 OBSERVATIONS

2.1 The sample stars

Our aim here was to investigate intrinsic polarization towards the end of the main sequence; specifically F, G and K types of which there are few examples in our previous surveys (Bailey et al. 2010; Cotton et al. 2016a,b). To do this effectively, we aimed for a polarimetric precision of less than 10 ppm per target. To achieve this in a time-efficient manner, we imposed a magnitude limit of 6.0 in selecting the programme stars. The mean precision finally achieved was 6.9 ppm, with the worst for any target being 10.1 ppm.

We selected the programme stars to cover the range of spectral types between F0 and K5. The K5 cut-off being a result of the imposed magnitude limit. We did not otherwise aim to favour stars with any particular properties and our initial target list consisted of the brightest accessible dwarf of each spectral type according to the types assigned to the stars of the *Hipparcos* catalogue (Perryman et al. 1997) in the VizieR database. An additional five K dwarfs were then added to achieve an even number of F, G and K types. Where scheduling or other constraints prevented a star of a particular type being observed, we selected another with a similar spectral type. Upon completion of our observations, we added five stars observed as part of a debris disc investigation programme not yet reported

(Marshall et al., in preparation). Some of these stars were on our original list of most preferred targets. The additional stars met the fundamental parameters of the study, being similarly bright, falling in the required spectral type range and having been observed to the same precision limits as the other programme stars.

The chromospheric emission at which a star is considered active is not universally defined and spans a range from mildly to very active, so the small number of stars surveyed here have been separated into just two groups according to their activity levels. We observed 10 stars that we could find classified as 'active' in the literature. These included several BY Dra variables, stars with emission-line spectral types, a flare star and the K dwarfs HD 191408 and GJ 785, the latter of which is listed in SIMBAD as 'Variable'. The classifications were not always consistent. Martínez-Arnáiz et al. (2010) classified HD 191408 as active but noted that it had been classified as inactive by other authors. Similarly, Jenkins et al. (2006) describes GJ 785 as active but Martínez-Arnáiz et al. (2010) describes it as inactive. Similarly, Procyon's status as an active star is somewhat controversial, it is described as an active star by Huber et al. (2011) through photometric and RV analysis but this is not supported by the classification given by Martínez-Arnáiz et al. (2010) in their spectroscopic work. For the purposes of this work, we refer to all of these stars collectively as active stars. As a result of the selection criteria and the way the programme was compiled, roughly even numbers of ordinary FGK dwarfs (14), inactive debris disc host stars (8) and active stars (10) were observed. For reasons that will be developed through the paper, we present the programme stars in these groupings in Table 1 and subsequently. Note that one star, ϵ Eri, is both active and a debris disc host, and we have grouped it with the active stars;[2] this will also be elaborated upon later.

2.2 Observation methods

Our observations were made with the HIPPI (HIgh Precision Polarimetric Instrument) mounted on the 3.9-m Anglo Australian Telescope (AAT). The AAT is located at Siding Spring Observatory near Coonabarabran in New South Wales, Australia. HIPPI was mounted at the f/8 Cassegrain focus of the telescope where it had an aperture size of 6.7 arcsec.

HIPPI is a high-precision polarimeter, with a reported sensitivity in fractional polarization of ∼4.3 ppm on stars of low polarization and a precision of better than 0.01 per cent on highly polarized stars (Bailey et al. 2015). HIPPI achieves its high precision by utilizing a ferroelectric liquid crystal (FLC) modulator at a frequency of 500 Hz to negate the effects of astronomical seeing. For the observations reported here, an SDSS g' filter was positioned, via a filter wheel, between the modulator and a Wollaston prism that splits the light into two orthogonal polarization states, which are then recorded separately by two photo multiplier tubes (PMTs). Second stage chopping to reduce systematic effects is accomplished by rotating the entire back half of the instrument after the filter wheel through 90° in an ABBA pattern, with a frequency that was adjusted, but was in the range of once per 40–80 s. An observation of this type measures only one Stokes parameter of linear polarization. To obtain the orthogonal Stokes parameter, the entire instrument is rotated through 45° and the sequence repeated. The rotation is performed using the AAT's Cassegrain instrument rotator. In practice, we also repeat the observations at geometrically redundant telescope position angles of 90° and 135° to allow the removal of instrumental polarization.

The effects of the background sky are removed through the subtraction of a 2 arcmin separated sky measurement that is acquired at each telescope position angle an object is observed in. The duration of the sky measurements was 3 min per Stokes parameter. The observing, calibration and data reduction methods are described in full detail in Bailey et al. (2015).

The g' band was chosen for our measurements mainly because it is the standard astronomical band in which HIPPI is most sensitive, to be consistent with Cotton et al. (2016a), and because bluer wavelengths are more sensitive to Rayleigh scattering that is most likely to be detected from exoplanets. The g' band is centred on 475 nm and is 150 nm in width, which results in the precise effective wavelength and modulation efficiency – the polarimeter's raw measurement for 100 per cent polarized light – changing with star colour. Table 2 gives the effective wavelength and modulation efficiency for various spectral types based on a bandpass model as described in Bailey et al. (2015). As all of our targets are within 30 pc, no interstellar extinction has been applied in the bandpass model. Our reported results apply the efficiency correction to each star measurement (a linear interpolation is used between the given types).

The observations were obtained predominantly over the course of two observing runs in the first semester of 2016; the first from February 25 to March 1, the second on June 26. A handful of serendipitously useful observations made for other programmes during earlier runs, but so far unreported, are also presented here. These data come from runs in 2015 May, June and October. The details of the conditions during those runs can be found in Cotton et al. (2016a) and Marshall et al. (2016).

The sky was cloudless for almost the entirety of the first semester 2016 run, with seeing that varied from around 1 arcsec to on rare occasions more than 6 arcsec, typically being between 2 and 4 arcsec. The seeing was similar in the 2015 runs. Of the second 2016 run, June 26 constituted the only clear night. The seeing was similar to that typically encountered in the previous run, but the last few observations were very slightly cloud affected. The effects of cloud were removed by determining the maximum signal during an observation, and rejecting integrations that fell below a threshold of 25 per cent of that. We have previously used this routine with a lower threshold (Cotton et al. 2016a), but raised it here because the targets are, on average, 2 mag fainter.

A number of stars with known high polarizations (∼1–5 per cent) were observed during each run, and used to determine the position angle zero-point; these were HD 80558 and HD 147084 in February–March, and HD 154445 and HD 147084 in 2016 June. The precision of each determination is less than 1°, based on the consistency of the calibration provided by the different reference stars that themselves have uncertainties of this order. A difference of ∼4° found between the two runs is related to the screw-fastening of the modulator being reset, and has been accounted for through the standard rotation formula.

The AAT is an equatorially mounted telescope, as such we use observations of stars previously measured with negligible polarizations to determine the zero-point or telescope polarization (TP). The adopted TP in 2015 May was $35.5 \pm 1.4 \times 10^{-6}$; for 2015 June, it was $36.5 \pm 1.2 \times 10^{-6}$ (Cotton et al. 2016a); for the 2015 October run, it was $55.9 \pm 1.1 \times 10^{-6}$ (Marshall et al. 2016). For the two 2016 runs reported here, the adopted TP was $20.6 \pm 1.8 \times 10^{-6}$.

[2] To avoid confusion, please note that we have both ϵ Eri and e Eri in this survey; e Eri is in the debris disc group.

Table 1. Properties of survey stars.

HD	HIP	Other names	V (mag)	$B-V$ (mag)	Spectral type	Sep[a] (arcsec)	Dist (pc)	RA (hh mm ss)	Dec (dd mm ss)	Galactic l (°)	Galactic b (°)	Notes[b]
Ordinary FGK swarfs												
10360	7751 B	p Eri A	5.96	0.88	K2V	11.22	7.8	01 39 47.6	−56 11 36	289.59	−59.67	
23754	17651	τ^6 Eri	4.20	0.45	F5IV-V		17.6	03 46 50.9	−23 14 59	217.35	−50.33	
30652	22449	π^3 Ori	3.19	0.44	F6V		8.1	04 49 50.4	06 57 41	191.45	−23.07	Var
38393	27072	γ Lep	3.60	0.47	F6V		8.9	05 44 27.8	−22 26 54	226.80	−24.27	
64096	38382	9 Pup	5.16	0.60	G0V[c]	0.62	16.5	07 51 46.3	−13 53 53	232.27	6.62	
102365	57443	HR 4523, 66 G Cen	4.88	0.67	G2V+M4V	22.99	9.2	11 46 31.1	−40 30 01	289.80	20.71	EP
102870	57757	β Vir	3.60	0.55	F9V		10.9	11 50 41.7	01 45 53	270.52	60.75	LP
114613	64408	GJ 501.2	4.85	0.70	G3V		20.7	13 12 03.2	−37 48 11	307.42	24.89	EP
119756	67153	i Cen	4.23	0.38	F2V	<0.01[d]	19.4	13 45 41.2	−33 02 37	315.85	28.47	
132052	73165	16 Lib	4.49	0.32	F2V		26.9	14 57 11.0	−04 20 47	351.73	46.27	
141004	77257	λ Ser	4.42	0.61	G0IV-V	([e])	12.1	15 46 26.6	07 21 11	15.69	44.10	
156384	84709	GJ 667	5.89	1.04	K3V+K5V[f]	1.82	6.8	17 18 57.2	−34 59 23	351.84	1.42	
197692	102485	ψ Cap	4.15	0.39	F5V		14.7	20 46 05.7	−25 16 15	20.00	−35.50	
209100	108870	ϵ Ind	4.69	1.06	K5V[g]		3.6	22 03 21.7	−56 47 10	336.19	−48.04	LP, PMS[h]
Debris disc host stars												
1581	1599	ζ Tuc	4.23	0.57	F9.5V		8.6	00 20 04.3	−64 52 29	308.32	−51.93	
10700	8102	τ Cet	3.50	0.72	G8.5V		3.7	01 44 04.1	−15 56 15	173.11	−73.44	HD
20794	15510	e Eri	4.27	0.71	G8V		6.0	03 19 55.7	−43 04 11	250.75	−56.08	HD, EP
20807	15371	ζ^2 Ret	5.24	0.60	G0V		12.0	03 18 12.8	−62 30 23	278.98	−47.22	
105211	59072	η Cru	4.15	0.32	F2V[i]	48.41	19.8	12 06 52.9	−64 36 49	298.18	−2.15	
109085	61174	η Crv	4.31	0.38	F2V		18.3	12 32 04.2	−16 11 46	296.18	46.42	Var
115617	64924	61 Vir	4.74	0.70	G7V		8.6	13 18 24.3	−18 18 40	311.86	44.09	EP
207129	107649		5.58	0.60	G2V		16.0	21 48 15.8	−47 18 13	350.88	−49.11	([j])
Active stars												
10361	7751 A	p Eri B	5.80	0.89	K5Ve[k]	11.22	7.8	01 39 47.6	−56 11 47	289.60	−59.66	
22049	16537	ϵ Eri[l]	3.73	0.88	K2V		3.2	03 32 54.8	−09 27 30	196.84	−48.05	BY, EP
26965	19849	o^2 Eri	4.43	0.82	K0.5V		5.0	04 15 16.3	−07 39 10	200.75	−38.04	Fl
61421	37279	α CMi, Procyon	0.37	0.42	F5IV-V+DQZ	4.85	3.5	07 39 18.1	05 13 30	213.70	13.03	BY
131156	72659	ξ Boo	4.59	0.78	G7Ve+K5Ve	7.32	6.7	14 51 23.4	19 06 02	23.09	61.35	BY
131977	73184		5.72	1.11	K4V		5.8	14 57 28.0	−21 24 56	338.24	32.67	BY
154417	83601	V2213 Oph	6.01	0.58	F8V		20.7	17 05 16.8	00 42 09	20.77	23.78	BY
165341	88601	70 Oph	4.03	0.86	K0V		5.1	18 05 27.3	02 30 00	29.89	11.37	BY
191408	99461		5.32	0.87[m]	K2.5V+M3.5	5.62	6.0	20 11 11.9	−36 06 04	5.23	−30.92	
192310	99825	GJ 785, 5 G Cap	5.72	0.91	K2V		8.9	20 15 17.4	−27 01 59	15.63	−29.39	Var, EP

Notes. [a]The separation of the listed companion from the primary in seconds of arc.
[b]BY: BY Dra variable, Fl: flare star, Var: variable, PMS: pre-main sequence, HD: hot dust, EP: exoplanet host system, LP: low polarization standard. All notes come from SIMBAD with the following exceptions: β Vir (Bailey et al. 2010), τ Cet (di Folco et al. 2007), e Eri (Ertel et al. 2014), Procyon (Schaaf 2008), ϵ Ind (Clarke 2010), Exoplanets from the NASA Exoplanet Archive (Akeson et al. 2013).
[c]Spectral type is for the combined light. The A and B components have V magnitudes of 5.61 and 6.49, and $B-V$ values of 0.61 and 0.81, respectively.
[d]Separation from Giuricin, Mardirossian & Mezzetti (1984).
[e]Listed in SIMBAD as a spectroscopic binary, but Duquennoy & Mayor (1991) suggest otherwise.
[f]A second companion with spectral type M1.5V is separated by 40.09 arcsec.
[g]A wide (416 arcsec) binary companion system consists of two brown dwarfs: ϵ Ind Ba (T1) and ϵ Ind Bb (T6) (McCaughrean et al. 2004).
[h]ϵ Ind A is a candidate for having an exoplanetary companion with a period of 30 yr (Zechmeister et al. 2013).
[i]Companion has a V magnitude of 11.8.
[j]HD 207129 is listed as a pre-main-sequence star in SIMBAD, however, its age is given elsewhere as 1.5–3.2 Gyr (Marshall et al. 2011).
[k]Spectral type from Glebocki, Musielak & Stawikowski (1980).
[l]In addition to being an active star, ϵ Eri is also a debris disc host. It is grouped with the active stars for reasons that will be developed through the paper.
[m]SIMBAD $B-V$ is unreliable for this star; we have substituted the data from Martínez-Arnáiz et al. (2010).

The AAT's primary mirror was re-aluminized the day before the beginning of the February–March run, eliminating the possibility of re-using calibration measurements made during earlier runs, but ensuring a clean surface. Preliminary calculations found the TP to be consistent within error between the February–March and June runs, and we have previously found good agreement between runs in the same semester. Consequently we combined the calibration measurements and applied them to both 2016 runs. This means that all but seven of the measurements reported here utilize the same zero-point. We used three calibration stars for the two runs, Sirius A which is only 2.6 pc distant, and β Hyi and β Vir that are at similar distances (∼10 pc) to the equatorial south and north, respectively. The error-weighted mean polarization was determined for each star, and then the average of the three stars adopted as the TP. The details of the individual observations are given in Table 3.

Table 2. Effective wavelength and modulation efficiency for different spectral types according to bandpass model.

Spectral type	Effective wavelength (nm)	Modulation efficiency (per cent)
B0	459.1	87.7
A0	462.2	88.6
F0	466.2	89.6
G0	470.7	90.6
K0	474.4	91.6
M0	477.5	92.0
M5	477.3	91.7

Table 3. Low polarization star measurements to determine TP for the 2016 February–March and June runs in the g' filter.

Star	Date	p (ppm)	θ (°)
Sirius A		18.0 ± 0.6	84.7 ± 1.7
	February 26	18.3 ± 0.8	87.0 ± 2.4
	February 26	18.4 ± 2.0	82.6 ± 6.6
	February 27	27.7 ± 3.7	83.1 ± 7.2
	February 28	17.1 ± 0.9	82.0 ± 2.9
β Vir		20.0 ± 4.1	79.3 ± 11.7
	February 26	18.6 ± 6.2	80.9 ± 19.4
	June 25	15.9 ± 8.9	88.0 ± 31.4
	June 25	24.9 ± 6.7	74.4 ± 15.6
β Hyi		24.1 ± 3.7	85.7 ± 9.0
	June 25	19.0 ± 9.0	106.8 ± 28.6
	June 25	26.6 ± 4.1	83.5 ± 8.8
Adopted TP		20.6 ± 1.8	83.3 ± 5.2

3 RESULTS

Table 4 gives the result for each star observed, as well as duplicate measurements of the same star below the aggregate parameters. The magnitude of linear polarization, p, is calculated for each star in column 7 in the usual way from normalized linear Stokes parameters q and u:

$$p = \sqrt{q^2 + u^2}. \tag{1}$$

Because polarization is always positive, it is a standard practice to debias it to best estimate the true value of p when calculating the mean of a group of stars with unrelated polarization angles. Following Serkowski (1962), debiasing is carried out according to:

$$\hat{p} \sim \begin{cases} \left(p^2 - \sigma_{\rm p}^2\right)^{1/2} & p > \sigma_{\rm p} \\ 0 & p \leq \sigma_{\rm p} \end{cases}, \tag{2}$$

where $\sigma_{\rm p}$ is the error in polarization. Column 11 in Table 4 gives the debiased polarization for each star. For stars with multiple measurements, q and u are first calculated from error-weighted means of the individual q and u observations, with p, $\hat{p}$ and polarization angle (θ) calculated from the means.

Polarization angles are calculated as:

$$\theta = \frac{1}{2} \arctan\left(\frac{u}{q}\right). \tag{3}$$

The calculation of the error in polarization angle, σ_θ, depends on the signal-to-noise ratio, $p/\sigma_{\rm p}$. If it is large, then the probability distribution function for θ is Gaussian, and 1σ errors (in degrees) are given by Serkowski (1962):

$$\sigma_\theta = 28.65\sigma_{\rm p}/p. \tag{4}$$

However, when $p/\sigma_{\rm p} < 4$, the distribution of θ becomes kurtose with appreciable wings. In such cases, equation (4) is no longer strictly accurate and instead, we make use of the work of Naghizadeh-Khouei & Clarke (1993) who give precisely σ_θ as a function of $p/\sigma_{\rm p}$ in their fig. 2(a).

4 DISCUSSION

4.1 Preliminary statistical analysis

The most basic analysis possible for identifying intrinsic polarization in this type of polarimetric survey is a straight comparison of the mean polarization of two or more groups of star systems. We have done this here for a number of different categories of objects, looking at the mean debiased polarization, $\hat{p}$, taking account of the increased interstellar polarization with distance through a simple division to give $\hat{p}/d$.

Any such analysis is confounded to a degree by interstellar polarization. All the stars observed are within ∼25 pc of the Sun, and the majority are within 10 pc. Consequently, we would expect that the interstellar contribution to the total polarization of a given sample be small, and that in ppm pc^{-1} for randomly distributed samples, the contribution should be fairly consistent. Despite this, without determining the direction of interstellar polarization, it cannot be subtracted, and we are left with the vector sum of intrinsic ($p_\star$) and interstellar (p_i) components. However, for a large enough sample of intrinsically polarized stars, we can expect the mean polarization to be greater than the interstellar polarization alone. Furthermore, if $p_\star > 2p_i$, then the total polarization will always be greater than the interstellar polarization alone. The statistics are described in more detail with the aid of diagrams in Cotton et al. (2016a) or Clarke (2010).

In Table 5, we calculated the mean polarization from the primary stellar groupings as presented in Table 1. From Table 5, it is clear that active stars are more highly polarized than inactive stars. This is an important finding, and we set it aside for detailed discussion in Section 4.6, where we examine the active stars in detail. In the remainder of this section, we look for other trends in the inactive stars only.

Table 5 does not reveal any significantly different polarization for debris disc host stars compared to ordinary FGK dwarfs. In Cotton et al. (2016a), we found slightly higher polarizations for debris disc systems, and significant polarization has been seen in a number of debris disc systems with aperture techniques (Hough et al. 2006; Wiktorowicz & Matthews 2008), so this is somewhat surprising. However, the stars examined here are on average much closer, meaning that in many cases, the debris disc might be wholly outside HIPPI's 6.7 arcsec diameter aperture, or may only have a fraction inside it. In addition, the polarization of debris disc systems is complicated and depends upon a number of parameters including disc radius, extent and inclination, as well as the optical properties of the dust grains in the disc (e.g. Graham, Kalas & Matthews 2007; Schüppler et al. 2015). This requires an in-depth analysis on a system-by-system basis, which we carry out in Section 4.5, but for the remainder of this section, we make no distinction between the debris disc stars and other inactive FGK dwarfs.

Other less likely scenarios for intrinsic polarization are examined in Table 6. None of the comparisons produced differences of any significance beyond 1σ.

If there is any material entrained between a binary pair, we might expect to see a polarization signal, as is the case for young close binaries (McLean 1980). η Cru is a binary debris disc system.

Table 4. HIPPI linear polarization measurements.

Name	HD	Obs.	Date (dd/mm/yy)	UT (hh:mm)	Exp. (s)	q (ppm)	u (ppm)	p (ppm)	θ (°)	$\hat{p}^a$ (ppm)
Ordinary FGK dwarfs										
p Eri A	10360	1	2016/03/01	10:03	1480	−6.6 ± 9.8	1.1 ± 10.5	6.7 ± 10.1	85.4 ± 38.5	0.0
τ^6 Eri	23754	1	2016/02/26	11:56	640	−1.3 ± 6.9	−16.8 ± 6.7	16.8 ± 6.8	132.8 ± 13.2	15.4
π^3 Ori	30652	1	2016/02/28	10:10	640	−3.5 ± 4.6	−6.2 ± 4.6	7.1 ± 4.6	120.4 ± 23.1	5.4
γ Lep	38393	1	2016/02/26	12:34	640	0.3 ± 5.6	−8.2 ± 5.5	8.2 ± 5.5	136.0 ± 24.1	6.0
9 Pup	64096	1	2016/02/29	13:01	1280	6.9 ± 6.6	−8.0 ± 6.6	10.6 ± 6.6	155.5 ± 22.3	8.2
HR 4523	102365	1	2016/02/28	16:29	1024	−10.6 ± 6.6	5.7 ± 6.6	12.0 ± 6.6	75.9 ± 19.4	10.1
β Vir	102870[b]	3			1920	1.3 ± 4.2	2.5 ± 4.2	2.9 ± 4.2	31.3 ± 38.2	0.0
			2016/02/26	17:37	640	2.3 ± 6.5	1.1 ± 6.5			
			2016/06/25	08:43	640	4.1 ± 9.2	−3.6 ± 8.9			
			2016/06/25	09:10	640	−1.3 ± 6.9	8.1 ± 7.1			
GJ 501.2	114613	1	2016/06/25	10:13	1024	−21.5 ± 7.7	31.0 ± 7.6	37.7 ± 7.7	62.3 ± 5.9	36.9
i Cen	119756	1	2016/06/25	09:44	640	−16.9 ± 7.4	19.8 ± 7.4	26.0 ± 7.4	65.2 ± 8.4	25.0
16 Lib	132052	1	2016/02/27	17:22	640	8.6 ± 6.9	0.4 ± 6.8	8.7 ± 6.9	1.2 ± 27.5	5.3
λ Ser	141004	1	2016/02/26	17:10	640	1.4 ± 8.5	12.8 ± 8.8	12.9 ± 8.7	42.0 ± 23.9	9.5
GJ 667	156384	1	2016/03/01	18:01	2560	5.2 ± 7.6	−1.5 ± 7.7	5.4 ± 7.6	172.2 ± 37.5	0.0
ψ Cap	197692	1	2016/06/25	15:01	800	−12.9 ± 7.3	−13.2 ± 8.4	18.5 ± 7.8	112.8 ± 14.1	16.8
ϵ Ind	209100	1	2016/06/25	13:33	1280	4.1 ± 9.0	−7.7 ± 8.8	8.7 ± 8.9	149.0 ± 32.4	0.0
Debris disc host stars										
ζ Tuc	1581	1	2016/06/25	17:17	640	−11.0 ± 6.8	11.4 ± 6.8	15.8 ± 6.8	67.0 ± 14.3	14.3
τ Cet	10700	2			1920	1.3 ± 3.1	0.3 ± 3.0	1.4 ± 3.0	7.0 ± 42.8	0.0
			2016/06/26	18:28	1280	−0.8 ± 4.1	8.0 ± 4.1			
			2016/10/20	14:20	640	4.2 ± 4.8	−8.3 ± 4.3			
e Eri	20794	1	2016/02/29	12:27	800	2.3 ± 6.5	4.6 ± 6.8	5.2 ± 6.7	31.6 ± 36.2	0.0
ζ^2 Ret	20807	1	2016/02/28	11:58	1120	8.2 ± 7.9	3.9 ± 8.5	9.1 ± 8.2	12.7 ± 30.1	3.8
η Cru	105211	1	2016/06/26	08:36	640	−16.8 ± 6.2	12.1 ± 6.3	20.7 ± 6.3	72.2 ± 9.0	19.7
η Crv	109085	1	2016/05/24	12:39	640	−4.7 ± 7.8	9.9 ± 8.0	11.0 ± 7.9	57.7 ± 25.3	7.6
61 Vir	115617	1	2016/06/26	10:54	960	−2.2 ± 7.2	−2.4 ± 7.2	3.3 ± 7.2	114.0 ± 42.6	0.0
HD 207129	207129	1	2016/06/26	19:11	1280	−27.9 ± 8.1	−6.3 ± 8.0	28.6 ± 8.0	96.3 ± 8.3	27.4
Active stars										
p Eri B	10361	1	2016/02/26	11:07	2560	0.5 ± 7.5	−42.2 ± 7.4	42.2 ± 7.5	135.3 ± 5.1	41.5
ϵ Eri[c]	22049	1	2016/02/26	10:24	640	28.4 ± 5.6	−12.0 ± 5.7	30.8 ± 5.7	168.5 ± 5.3	30.3
o^2 Eri	26965	1	2016/02/29	09:51	1024	4.5 ± 6.0	−19.3 ± 6.0	19.9 ± 6.0	141.6 ± 9.0	18.9
Procyon	61421	3			1280	4.7 ± 1.5	−5.8 ± 1.5	7.5 ± 1.5	154.5 ± 5.8	7.3
			2016/10/20	18:14	320	12.7 ± 3.1	−1.2 ± 3.1			
			2016/02/29	13:32	640	1.4 ± 2.2	−10.8 ± 2.2			
			2016/03/01	09:25	320	3.6 ± 2.6	−2.0 ± 2.7			
ξ Boo	131156	2			2304	45.8 ± 5.2	3.0 ± 5.2	45.9 ± 5.2	1.9 ± 3.2	45.6
			2016/02/26	18:07	1024	40.1 ± 8.9	−2.6 ± 9.0			
			2016/02/29	18:07	1280	48.8 ± 6.4	5.8 ± 6.4			
HD 131977	131977	1	2016/02/26	16:26	2560	4.6 ± 8.2	22.8 ± 8.0	23.2 ± 8.1	39.3 ± 10.8	23.2
V2213 Oph	154417	1	2016/06/25	11:05	2560	3.7 ± 8.3	19.8 ± 8.5	20.1 ± 8.4	39.7 ± 13.8	18.3
70 Oph	165341	1	2016/02/27	18:16	640	−29.0 ± 9.4	−17.3 ± 8.8	33.8 ± 9.1	105.4 ± 7.9	32.5
HD 191408	191408	1	2016/06/25	12:30	1680	−15.1 ± 9.3	−20.7 ± 8.5	25.6 ± 8.9	117.0 ± 10.7	24.0
GJ 785	192310	1	2016/06/25	15:49	2560	−18.4 ± 6.9	2.9 ± 6.8	18.7 ± 6.9	85.5 ± 11.6	17.4

Notes. [a] $\hat{p}$ is debiased polarization; see the text of Section 3 for details.
[b] β Vir was used as a low polarization standard.
[c] ϵ Eri also hosts a circumstellar debris disc.

Table 5. Mean polarization for primary stellar groupings.

Group	N	Mean d (pc)	Mean $\hat{p}$ (ppm)	$\hat{p}$/d (ppm/pc)
Ordinary FGK Dwarfs	14	13.1	9.9 ± 1.9	0.8 ± 0.1
Debris disc Host Stars	8	11.6	9.1 ± 2.5	0.8 ± 0.2
Active Stars	10	7.3	25.8 ± 2.2	3.5 ± 0.3
All inactive stars[a]	22	12.6	9.4 ± 1.4	0.8 ± 0.1

Note. [a]Includes both debris disc hosts and ordinary FGK dwarfs.

The binary debris disc system ϵ Sgr is thought to display elevated levels polarization as a result of the secondary illuminating part of the disc, creating an asymmetry in aperture measurements (Cotton et al. 2016c). When we consider all the binary stars as a group, Table 6 does not reveal any systematic increase in polarization through such mechanisms in the FGK dwarfs we observed.

For completeness, we have also examined the difference between known exoplanet hosts and non-exoplanet hosts. Particularly close hot-Jupiters have the potential to induce a detectable polarization signal (Seager et al. 2000). It has also been proposed that the

Table 6. Mean polarization for other groupings of inactive stars.

Group (Inactive)	N	Mean d (pc)	Mean $\hat{p}$ (ppm)	$\hat{p}/d$ (ppm pc^{-1})
Single	15	12.3	9.7 ± 1.6	0.8 ± 0.1
Binary/multiple[a]	7	13.1	9.5 ± 2.9	0.7 ± 0.2
Binary in aperture	3	14.2	11.1 ± 4.2	0.8 ± 0.3
Exoplanet hosts	4	11.1	11.7 ± 3.5	1.1 ± 0.3
Non-exoplanet hosts	18	12.7	9.1 ± 1.7	0.7 ± 0.1
F-type	10	15.3	11.5 ± 2.1	0.8 ± 0.1
G-type	9	11.6	10.7 ± 2.4	0.9 ± 0.2
K-type	3	7.0	0.0 ± 5.2	0.0 ± 0.8

Note. [a]This line gives the binaries/multiples as identified in Table 1; the following line includes only those binaries contained wholly within the aperture: 9 Pup, i Cen and GJ 667.

presence of a close in giant planet induces magnetic activity in the host star – which might induce polarization – though an attempt to observe this effect did not produce a positive result (Cuntz, Saar & Musielak 2000). None of the systems observed are known to host a sufficiently large and close planet to enact either of these mechanisms. It is extremely unlikely that any such planet would be undiscovered in a system less than ∼25 pc from the Sun (but not impossible if it were in a face-on orbit or if the system specifics make it a challenging radial velocity target). Table 6 indicates a slightly elevated polarization for the exoplanet host stars, but only at barest 1σ significance. The most plausible explanation for this level of difference in the polarization signal of the two groups is the combination of a small sample size and variability in interstellar polarization.

Tinbergen & Zwaan (1981) suspected the presence of variable intrinsic polarization at the 100 ppm level in stars with spectral type F0 and later. More recently, Cotton et al. (2016a) combined their measurements with those of Bailey et al. (2010) to reveal greater polarizations in M-type stars at about that level. The data also suggested slightly elevated levels in F, G and K types over A-type stars. However, the later studies contained a combined total of only three dwarf stars later than A9, and the conclusions regarding later types were restricted to the giant class. In Table 6, we compared the polarizations of F, G and K types. The table contains only inactive stars. Most of the active stars are K-type stars (with only a couple of earlier types) and, if included, would show much higher polarizations for K types. As it is, all three of the inactive K-type stars have a debiased polarization of zero, which does not make for good statistics. The table does not reveal any trends with spectral type. None the less, we take a closer look at ordinary FGK dwarfs in Section 4.4.

4.2 Interstellar polarization

Interstellar polarization is of interest for what it can tell us about the composition and history of the ISM and the Interstellar Magnetic Field (ISMF) (Frisch & Schwadron 2014; Heiles 1996). In combination with gas density studies such as those of Lallement et al. (2003) and Redfield & Linsky (2008), polarimetry is the best tool we have for understanding the composition of the ISM close to the Sun. The dust density of the ISM may also play a role in planet formation, and Helled et al. (2014) have called for the development of giant planet formation models that incorporate the initial size distribution of interstellar dust grains. Accurate dust maps will be required to test such models. Recently it has been hypothesized that the atmosphere of Mars was stripped through interactions with interstellar clouds (Atri 2016). So, mapping interstellar polarization may also tell us about the likely habitability of planets in nearby space.

In Section 4.1, $\hat{p}/d$ amongst inactive stars was very similar no matter the exact grouping. The basic statistics therefore suggest that the inactive stars in our data set have a polarimetric signal dominated by interstellar polarization. Their measurement thus represents valuable data on the ISM close to the Sun. However, the analysis so far has only looked at groups of stars, which can lead to individual stars with significant levels of intrinsic polarization being missed. Our first step in exploring the data in this context is to repeat the exercise conducted in Marshall et al. (2016). In Fig. 1, we have plotted $\hat{p}/d$ for each inactive star along with those from the literature thought to be polarized only by the ISM with comparable errors.

The literature data plotted represent all non-peculiar, non-debris disc, inactive A–K type stars (except α Tuc and δ Sgr that are believed to be intrinsically polarized) from the HIPPI (Bailey et al. 2015; Cotton et al. 2016a,b) and PlanetPol (Bailey et al. 2010) bright star surveys, along with the control stars from Marshall et al. (2016)'s work on hot dust. We refer to these stars collectively as the *Interstellar List*. A full list of the additional stars representative of the ISM and their adopted polarizations is supplied in Appendix A. None of these stars belong to types known to be intrinsically polarized in the waveband of their measurement, and statistical tests very similar to those carried out in Section 4.1 have been used to deduce only interstellar polarization (Bailey et al. 2010; Cotton et al. 2016a). Where we have measurements in multiple bandpasses, the g' measurement is used; for the PlanetPol observed stars, we have multiplied the polarization by 1.2 in accordance with the polarimetric colour of the local ISM determined in Marshall et al. (2016). It should be noted that the polarimetric colour determination, though the best available, has a very large error associated with it, and more multiband measurements of nearby stars are badly needed. A couple of the stars from the HIPPI survey have been re-observed as part of calibration procedures for later runs, and for these, we have updated measurements.

The new data help to fill out the plot compared to the Marshall et al. (2016) work, even whilst we exclude a number of debris disc objects included previously. Of the 22 stars newly plotted on the diagram, only one really stands out as being against trend: the debris disc system ζ^2 Ret is underpolarized compared to the surrounding stars. Debatably, there are other debris disc systems (marked on the plot with horizontal bars) that might also be identified as over or underpolarized, but the apparent clumpiness of the ISM on this scale does not lend itself to firm identifications. We discuss the debris disc systems in more detail in Section 4.5 after subtracting interstellar components in Section 4.3. However, for the remainder of this section dealing with interstellar polarization, we remove all but two: e Eri – that has a tiny infrared excess (see Section 4.5), and η Crv – where the aperture is wholly inside the cold component of the disc.[3] For these reasons, e Eri and η Crv are essentially ordinary FGK dwarfs as far as HIPPI observations are concerned. Thus, we have a total of 16 stars that have met the same criteria as the others on the interstellar list, which we use to describe the local ISM.

The most striking feature of Fig. 1 is the region of lower polarization in the Northern hemisphere. This region roughly corresponds

[3] There is a warm inner disc component as well, but this is dominated by small grains and likely to be very weakly polarizing at the wavelengths of interest here.

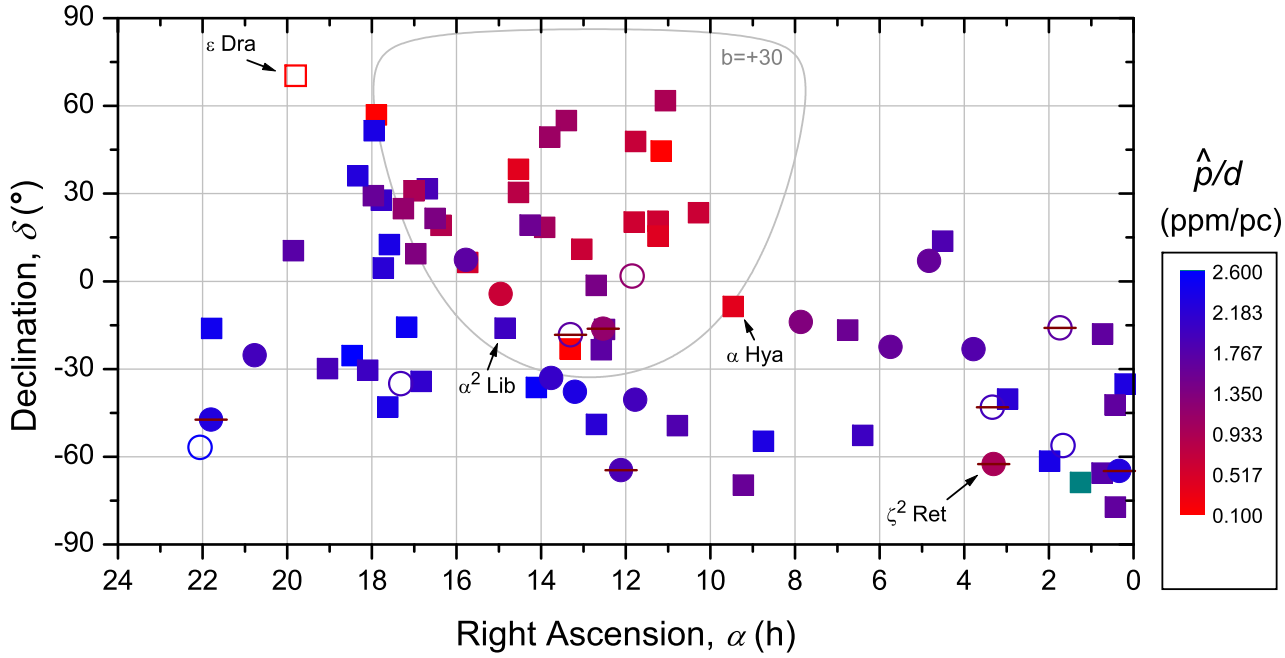

Figure 1. Plot of polarization/distance ($\hat{p}/d$) versus sky position for stars within 100 pc (most are within 50 pc). The new measurements added by this work are shown as circles. Literature measurements, shown as squares, are taken from (Bailey et al. 2010, 2015; Cotton et al. 2016a,b; Marshall et al. 2016). Only those stars believed to have negligible intrinsic polarization have been included. The PlanetPol values have been scaled to g' according to the mean colour of the ISM determined from g' and r' measurements using Serkowski's Law; see Marshall et al. (2016) for details. Debris disc stars are indicated by a horizontal brown bar. The data point colour scale running from red to blue corresponds to 0.1–2.6 ppm pc^{-1} in a logarithmic fashion. Data points that debias to zero are shown as open symbols, with their colour representing the 1-sigma error. The cyan data point is HD 7693 that has a $\hat{p}/d$ value of 7.5 ppm pc^{-1}. The grey line corresponds to $b = +30^\circ$.

to the projected area north of $+30^\circ$ galactic latitude. Though there are a few stars that appear to fall just on the wrong side of this boundary – ϵ Dra, α^2 Lib and α Hya – which we have marked on the plot. This is not unexpected; the ISM is likely to be clumpy on this scale, and the $+30^\circ$ galactic latitude line is an arbitrary boundary. Indeed, our results are not inconsistent with those of Tinbergen (1982), who identified what he called the 'local patch' – a region of dustier ISM centred on $l = 0$, $b = -20$. The existence of this feature was brought into question by Leroy (1993), but is supported by the work of Frisch et al. (2012).

4.2.1 *Polarization with distance*

For the purpose of determining trends in polarization against distance, $\hat{p}/d$, for the groups of stars north and south of $b = +30$, we have plotted them in Fig. 2 in different shades – grey for $b > +30$ and black for $b < +30$. A zoomed-in version showing only stars within 30 pc is shown in Fig. 3. The border region stars ϵ Dra and α Hya though plotted as $b < +30$ in Fig. 2 are used in the calculation of the $b > +30$ trend line. HD 7693 – which appears a remarkably local phenomena – has been excluded from the calculation, as has α^2 Lib. We have excluded α^2 Lib not just on account of its border status, but also because its polarization direction appears anti-aligned to surrounding stars in Fig. 4, leading us to suspect intrinsic polarization.[4] We also exclude HD 28556 on account of its large error. For the $b > +30$ group of stars, the fitted linear trend is 0.261 ± 0.017 ppm pc^{-1}. For the $b < +30$ group, we initially calculate 1.318 ± 0.041. These trends being fairly similar to those presented in Cotton et al. (2016a) and Bailey et al. (2010).

However, upon plotting the determined linear trend for the $b < +30$ group, it became clear that the closest stars were not well described by this simple relation. We further noted that the trend in polarization with distance for $b < +30$ stars is greater than the mean polarization with distance for inactive stars given in Table 5. Only 4 of the 22 inactive stars observed for this work belong to the $b > +30$ region, and so this does not fully explain the discrepancy. Previously (Cotton et al. 2016a), we reported that $\hat{p}/d$ seemed to be elevated between 10 and 30 pc towards the galactic south, but this elevated polarization region actually looks a bit narrower now – closer to 15 to 25 pc. The mean distance of the inactive stars observed here is only 12.6 pc, so there are many closer stars. Examination of Fig. 2 suggests that within 8.5 pc of the Sun, there is very little interstellar polarization. There is a very strong possibility that this is an artefact of the debiasing, given that our median precision in this study is 7.0 ppm. Models of the Loop I Superbubble (see Section 4.2.2) place the Sun on or near its rim (Frisch & Schwadron 2014). However, it does seem unlikely that the Sun would sit exactly on the border between two regions with different p/d relations, hypothesizing a smoother transition between the two regions seems reasonable. According to Frisch et al. (2012, 2010), the ISM has a very low density within 10 pc, and, in this region, is partially ionized, which indicates tight coupling of gas and dust densities, and therefore very low dust densities as well. For the $b > +30$ group of stars, if we fit a linear trend restricted to within 14.5 pc, then the fit is 0.800 ± 0.120 ppm pc^{-1}, which, at a distance of 14.5 pc, corresponds to 11.6 ± 1.7 ppm; then for the $b > +30$ stars beyond that, the slope of their polarization is given

[4] Looking at this object in detail is beyond the scope of this work, but we are making follow-up observations with our mini-HIPPI instrument (Bailey, Cotton & Kedziora-Chudczer 2017) designed for small telescopes.

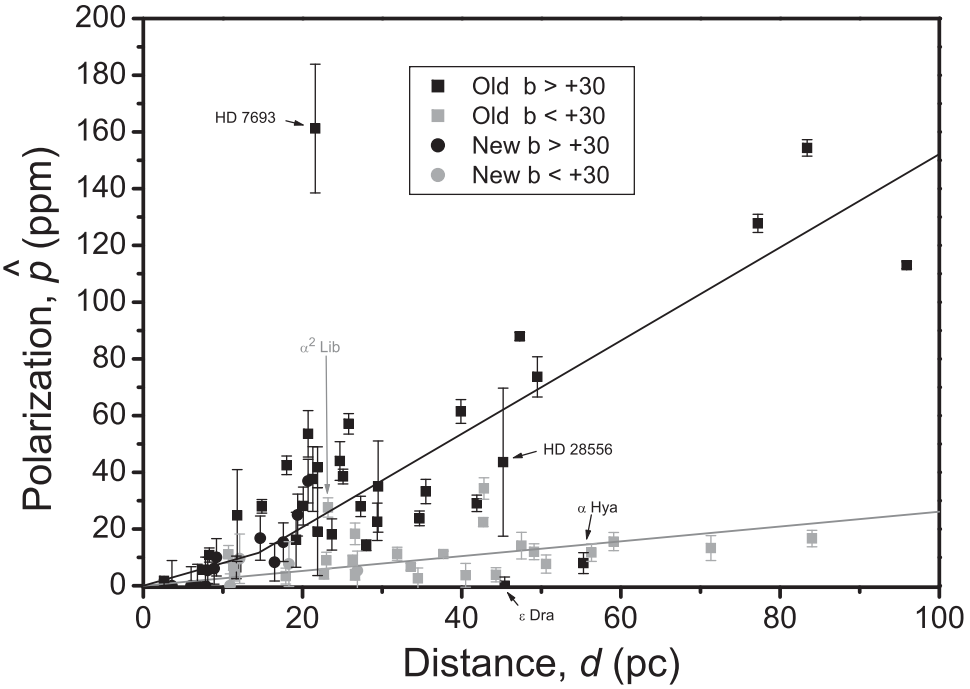

Figure 2. Debiased polarization with distance for the inactive non-debris disc stars observed in this work (circles), and those from other works believed to represent interstellar polarization (squares) within 100 pc. Stars with galactic latitude greater than 30° are plotted in grey, and the remainder in black. The lines of the same colour are linear and piece-wise linear fits to the data, respectively. Stars discrepant with the apparent trends mentioned in the text are marked on the plot.

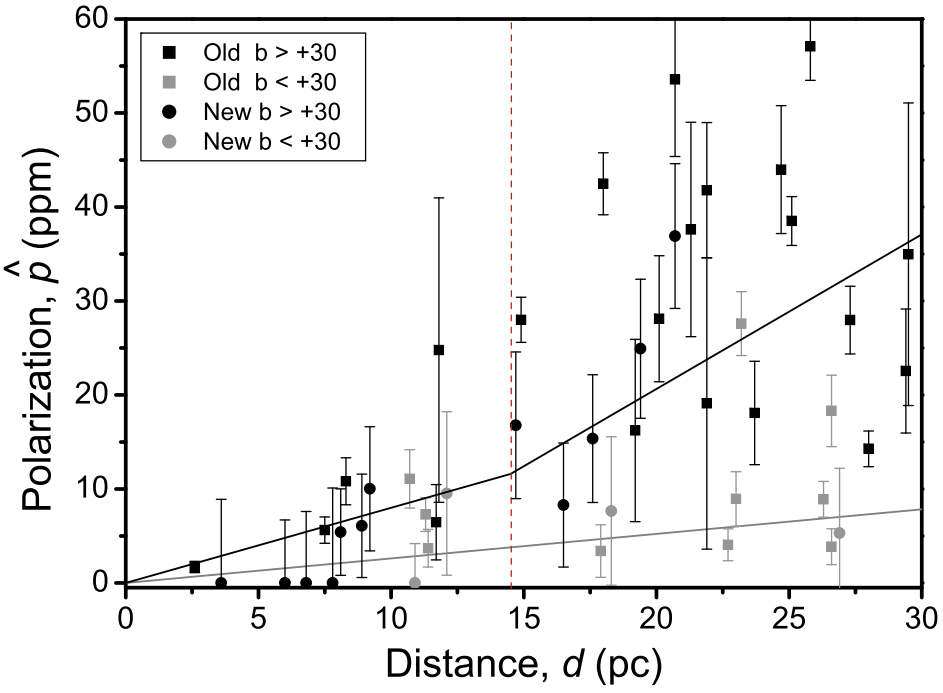

Figure 3. As per Fig. 2 but zoomed in to within 30 pc to best show the new data stars for this work, which are all within ∼25 pc. Debiased polarization with distance for the inactive non-debris disc stars observed in this work (circles), and those from other works believed to represent interstellar polarization (squares). Stars with galactic latitude greater than 30° are plotted in grey, and the remainder in black. The lines of the same colour are linear and piece-wise linear fits to the data, respectively. The red dashed line marks 14.5 pc distance.

by 1.644 ± 0.298 ppm pc^{-1}. We adopt this relation to describe the interstellar polarization in later in Section 4.3. The division between the two polarizations with distance regimes is marked on Fig. 3.

Figs 2 and 3 emphasize the greater scatter amongst the $b < +30$ group compared to the $b > +30$ group. This is to be expected, given that it represents a larger volume of space. However, there may be other factors at play. Of the $b > +30$ group, a large portion

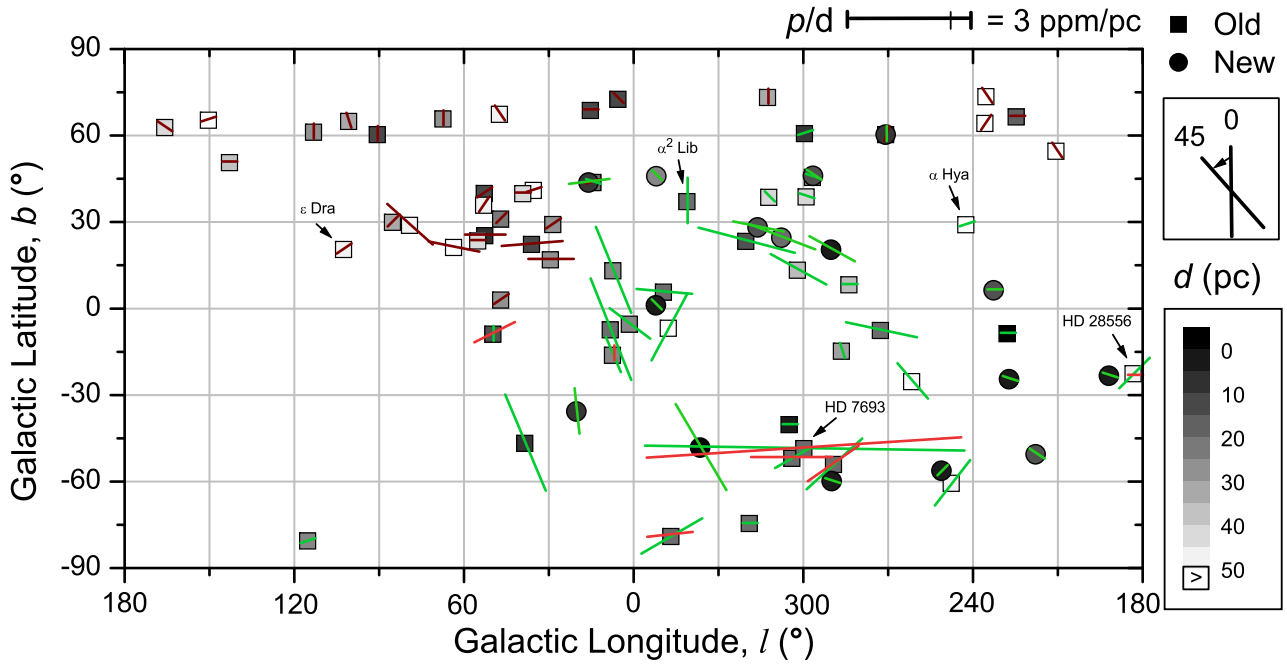

Figure 4. Plot of polarization/distance (p/d) versus position in galactic co-ordinates for stars within 100 pc (most are within 50 pc). The directions of the pseudo-vectors give the measured galactic polarization angle, θ_G. The new measurements added by this work are shown as circles. Literature measurements, shown as squares, are taken from Bailey et al. (2015), Cotton et al. (2016a), Cotton et al. (2016b), Marshall et al. (2016) and Bailey et al. (2010). The vector colours are representative of the bandpasses the original measurements were made in: green for g', red for r' and wine for PlanetPol's red bandpass. The minimum vector length corresponds to 0.5 ppm pc^{-1}, longer vectors are representative of the polarization with distance.

are the stars measured with PlanetPol at redder wavelengths and scaled to g'. If weak polarigenic mechanisms are stronger or more prevalent at bluer wavelengths, this could explain the increased scatter in the $b < +30$ group. For instance, there are a number of K-giants amongst the literature stars plotted. Amongst them, only Arcturus (data from PlanetPol) has been identified as intrinsically polarized, and then only in the B band (Kemp et al. 1986, 1987a). However, M-giants as well as K- and M-supergiants with dust in their atmospheres show intrinsic polarization that increases as $1/\lambda$ (Dyck & Jennings 1971). This behaviour may also be present in K-giants at lower levels (Cotton et al. 2016a,b). So, it is more likely that g' measurements of K giants are contaminated by small levels of intrinsic polarization. Similarly, stellar activity models show a stronger signature at bluer wavelengths (Saar & Huovelin 1993), and could potentially contribute to greater scatter in the HIPPI g' measurements of *nominally* inactive stars.

4.2.2 *The interstellar magnetic field close to the Sun*

In work examining the interstellar magnetic field, it is common to plot polarization vectors in galactic co-ordinates, which we do in Fig. 4. Here the polarization angle has been rotated into galactic co-ordinates using the method outlined by Stephens et al. (2011). In this projection, the polarization angle probes the magnetic structure of the local ISM.

Close to the Sun, there are two main large-scale components of the ISMF. There is a uniform large-scale magnetic field aligned parallel to the Galactic plane towards $l = 82.8$, and a local magnetic structure known as Loop I (or the Loop I Superbubble; Frisch & Schwadron 2014). The Loop I Superbubble results from stellar winds and supernovae explosions in the ScoCen association in the last ∼15 Myr (de Geus 1992; Frisch 1995, 1996; Heiles 2009). During the expansion of the Loop I Supperbubble, the ISMF has been swept up, creating a magnetic bubble-like structure that has persisted through the late stages of its evolution (Tilley, Balsara & Howk 2006). If Loop I is a spherical feature, the Sun sits on or near its rim (Frisch 1990; Heiles 1998). Optical polarization and reddening data show that the eastern parts of Loop I, $l = 3$–60, $b > 0$, fall within 60 to 80 pc of the Sun (Frisch, Redfield & Slavin 2011; Santos, Corradi & Reis 2011).

Frisch et al. (2012, 2015) have conducted perhaps the most comprehensive study of optical polarization close to the Sun, agglomerating the PlanetPol data with a number of other data sets going back to the 1970s. That work is ongoing with an update due shortly (Frisch, private communication). The data set we present here is far less comprehensive and using it to revisit their work is beyond the scope of this paper. However, our data do contain more observations within 50 pc of the Sun, especially at southern latitudes. Distance information for each star is encoded in a grey-scale colour bar in Fig. 4, and it can be seen that all but a handful are within 50 pc. On this scale, we do not see the ridge of the Loop I superbubble traced out by polarization vectors in the same location as other studies looking at greater distances (for comparison, see fig. 7 of Salter 1983 that traces this structure in the vectors of 50–100 pc stars). Our results appear fairly consistent with the direction of the local interstellar magnetic field within 40 pc determined by Frisch et al. (2012). Their weighted best fit gives the position of the magnetic north pole to be $l = 47 \pm 20°$, $b = 25 \pm 20°$.

In Fig. 4, the vectors have been rendered in colours representative of the bandpasses of the original measurements. Demonstrably, there is presently insufficient overlapping data in different bands to gain a good understanding of any dispersion due to the ISM. In general though, the trends in vector direction appear to be similar for the measurements made with the different instruments.

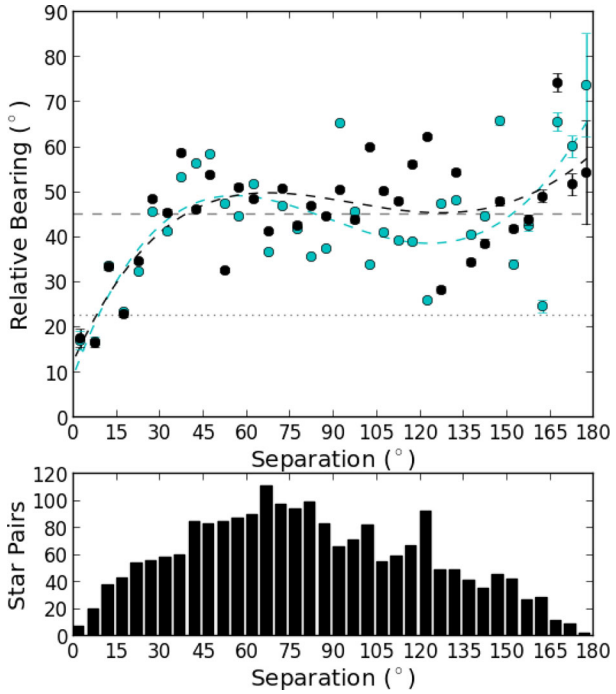

Figure 5. Upper panel: plot of the relative bearings of stars within 50 pc, binned per 5°. Data are taken from Cotton et al. (2016a), Cotton et al. (2016b), Marshall et al. (2016) and Bailey et al. (2010). Black data points are relative bearing calculated from polarization angles, those in cyan from galactic polarization angles. The dashed trend lines are the fourth-order polynomials drawn to guide the eye. Lower panel: a histogram showing the number of star pairs binned per point in the upper panel.

Although it is impractical to plot the polarization angle error, it is worth noting that the errors are larger for the closer stars on account of them being less polarized by the ISM. Despite this, there is a high degree of coincidence in the polarization angles of stars with their 2D neighbours, and no obvious discrepancy with distance. It is a common practice in astronomical polarimetry to make measurements of nearby control stars to determine the interstellar polarization, and then subtract this from the target's measured polarization (Clarke 2010). Near the Sun, it can be at times very difficult to identify sufficiently close control stars. With this in mind, we have endeavoured to determine the scale over which the local interstellar magnetic field rotates the angle of interstellar polarization. To do this, we consider every star within 50 pc plotted in Fig. 4. We then measure the absolute difference in polarization angle between each star and every other star, which gives a value between 0° and 90° – for simplicity, we refer to this as the relative bearing. We then place the data into bins for each 5° separation between pairs of stars, taking the error-weighted mean for each bin. The result, both for galactic polarization angle and polarization angle (i.e. equatorial co-ordinates), is plotted in Fig. 5.

Statistically, for an ensemble of unrelated stars, the mean relative bearing will be 45°. For neighbouring stars, the interstellar magnetic field orientates them similarly, and we can see from Fig. 5 that within 35° separation, there is a fairly smooth increase in relative bearing with separation. Fitted fourth-order polynomials are plotted as indicative of the data trend. The trend lines do not pass through zero – but closer to 12.5 – for which there are probably a number of contributing factors. First, there are only 8 pairs in the first (0°–5°) bin and 25 in the second bin; the individual measurements also have some errors associated with them. Magnetic turbulence may also be a factor. Frisch et al. (2012) have previously determined a trend in polarization angle rotation with distance for the PlanetPol data within 16–20 h right ascension. Their best-fitting trend had a standard deviation about the line of 23° attributed to magnetic turbulence. The actual trend they determined amounted to ∼0.25 ° pc^{-1} that, over the 50 pc range of the data plotted here, amounts to 12.5°. All of these factors, together with any unidentified intrinsic or local effects, will be contributing to the deviation from zero.

In Fig. 5, there is a large amount of scatter around 45° relative bearing at larger separations. There is also a difference between using the polarization angle and the galactic polarization angle at large separations. The measure trend line calculated using the galactic polarization angle appears negatively correlated at the largest separations. This may be attributed to the unevenness of the distribution of data along with large-scale symmetry associated with the galactic magnetic field.

Table 7. A comparison of different methods for determining interstellar polarization angle.

Method	Mean difference (°)
Mean PA	30.3
Mean PA separation-weighted	29.1
Mean PA error-weighted	39.1
Mean PA distance-weighted	31.6
Mean GPA	30.0
Mean GPA separation-weighted	30.5
Mean Stokes per distance	50.6
Magnetic field	40.1

4.2.3 A simple method for determining the angle of interstellar polarization

We have a determination of the magnitude of interstellar polarization with distance from Section 4.2.1. To carry out a vector subtraction of interstellar polarization for each star, we also need a determination of the angle of interstellar polarization for each star. Fig. 5 shows there is a fair degree of correspondence between the polarization angles of neighbouring stars that we might use to make such a determination. In this section, we trial a number of different methods for determining the angle of interstellar polarization. To do this, we make use of the *interstellar list* that includes all the same stars as Fig. 5 within 50 pc. For each method, we calculate the difference in the angle determined for each star in the interstellar list with the angle actually measured, and decide on the best method using the mean difference (Table 7). A brief description of each method is as follows.

(i) Mean PA Method: the angle for each star is the mean of the polarization angles of all other stars in the *interstellar list* within 35° separation.

(ii) Mean PA Separation-Weighted Method: as for the Mean PA Method, but the individual polarization angles are weighted by angular separation as:

$$Wt = (1 - s_a/35), \quad (5)$$

where s_a is the angular separation in degrees. (The weighting approaches zero at 35° separation.)

(iii) Mean PA Error-Weighted Method: as per the Mean PA Method, but the individual angles are weighted according to the inverse of their square error.

(iv) Mean PA Distance-Weighted Method: as per the Mean PA Method, but the individual angles are weighted according to

$$Wt = \begin{cases} d_c/d_t & d_c > d_t \\ d_t/d_c & d_t > d_c \end{cases}, \quad (6)$$

where d_t is the distance to the target star and d_c the distance to the control star from the Sun.

(v) Mean GPA Method: as per the Mean PA Method, but the individual polarization angles are first transformed to galactic polarization angle to take the mean, before being transformed back to polarization angle.

(vi) Mean GPA Separation-Weighted Method: as per the Mean PA method separation-weighted method, but the individual polarization angles are first transformed to galactic polarization angle to take the mean, before being transformed back to polarization angle.

(vii) Mean Stokes per Distance Method: the q and u vectors in ppm pc^{-1} for each star in the interstellar list were averaged in this method. This essentially weighs the angles by the strength of the polarization with distance.

(viii) Magnetic Field Method: here we determine the direction of the magnetic field at each target star's sky position based on that derived by Frisch et al. (2012), and assume that the direction of the magnetic field lines corresponds to the polarization direction. Doing this involved transforming the lines of longitude in a magnetic field co-ordinate system to an equatorial co-ordinate system, which involved determining the longitude of the ascending node of the magnetic co-ordinate system from the plots in Frisch et al. (2012) as 43.°33.

Table 7 indicates that the mean PA separation-weighted method is the best, and so we adopt it in determining the interstellar polarization. This method is only slightly better than the mean PA method, which is completely unweighted. The reason the improvement is only slight has to do with the number of stars in the interstellar list, and, on many occasions, few being very close in terms of separation on the sky. This can lead to a determination being heavily weighted to one or two stars. Any star on the list could have an unidentified intrinsic component, be misaligned through magnetic turbulence, or be poorly constrained, and so it is better to average more stars. Statistically, stars with larger polarizations are more likely to have a large unidentified intrinsic component, and the especially poor performance of the mean Stokes per distance method suggests that there may be a number of these stars.

When we tried reducing the angular separation cut-off to less than 35°, the mean difference also increased because of a reduced number of control stars per target. Similarly, the mean PA distance-weighted method is worse because the statistical disadvantage of favouring a smaller number of control stars outweighs the distance weighting's advantage better accounting for rotation with distance. The mean PA error-weighted method is much worse than the mean PA method. Again, this is a consequence of differing error levels effectively reducing the number of control stars over which the average is taken.

The galactic polarization angle methods do not do significantly better than the polarization angle methods. Unlike on larger scales, the magnetic field probed by stars in nearby space probably does not correlate as closely to galactic co-ordinates. The magnetic field method might therefore be expected to do better, but does not on the whole. Examination of Fig. 6 shows that there are actually regions of the sky where this method is doing very well, and others where it is not. One likely explanation for this is that the error in the determination of the pole position is large – 20° in each direction.

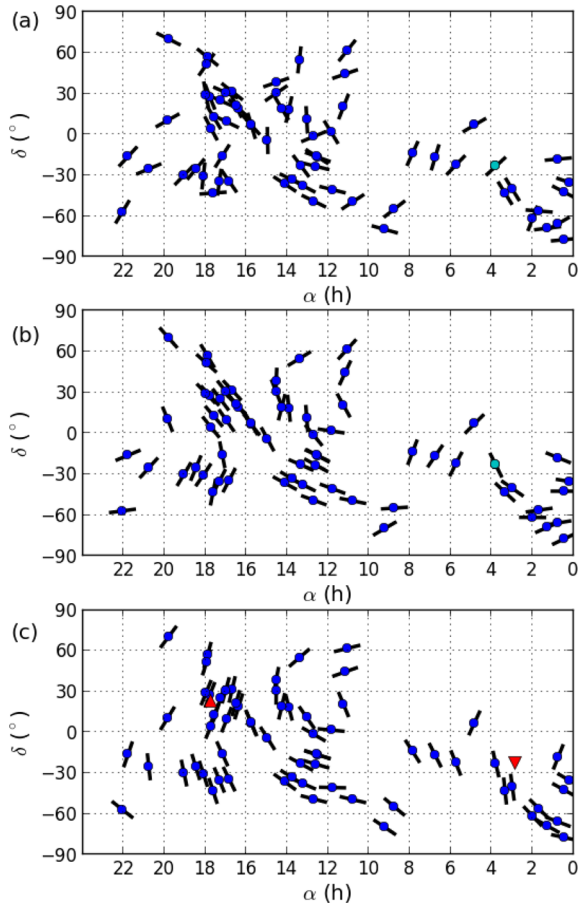

Figure 6. (a) The measured polarization angles of stars representing interstellar polarization within 50 pc. (b) The polarization angles determined for the interstellar polarization from the mean PA method. The cyan point in subplots (a) and (b) is τ^6 Eri (03^h 47 arcmin, $-23°$ 15 arcmin). (c) Polarization angles determined from the magnetic field method, based on Frisch et al. (2012). Here the magnetic north pole (up-pointing red triangle) is positioned at (265.°5, 23.°0) and the longitude of the ascending node is 43.°33; the south magnetic pole is shown as a down-pointing red triangle.

Frisch et al. (2012)'s determination had the high-precision PlanetPol data to work with, but little high-precision data at southern latitudes. This is evident in the figure where the agreement is much better near the north magnetic pole. There are potentially other significant contributors to the interstellar polarization direction too, not just the magnetic field, including, for instance, the IBEX ribbon (Frisch et al. 2010). In this instance, however, we are trying to obtain a simple method, and considering all the magnetic structure within the local ISM is beyond the scope of this work.

4.3 Interstellar subtraction

In this section, we have determined interstellar polarizations for each of the stars in our survey using the *p/d* relations determined in Section 4.2.1 and the mean PA method (Section 4.2.3). In the first instance, we treat our interstellar polarization determination as a model, neglecting the model uncertainties. This allows us to take the measurement errors for p as the errors in $p_\star$, and lets us calculate a debiased intrinsic polarization, $\hat{p}_\star$, for each object using equation (2). We then consider the influence of uncertainties in the model parameters on a case-by-case basis – in general, this is only necessary for the furthest stars in the $b < +30$ group.

Table 8. Interstellar and intrinsic polarization components of FGK dwarfs[a].

Name	HD	p	θ	p_i	θ_i (°)	$p_\star$	$\theta_\star$	$\hat{p}_\star$
Ordinary FGK dwarfs								
p Eri A	13060	6.7 ± 10.1	85.4 ± 38.5	6.3	98.3	2.9	15.4	0.0
τ^6 Eri	23754	16.8 ± 6.8	132.8 ± 13.2	16.7	134.1[b]	0.8	91.5	0.0
π^3 Ori	30652	7.1 ± 4.6	120.4 ± 23.1	6.5	135.1	3.5	87.8	0.0
γ Lep	38393	8.2 ± 5.5	136.0 ± 24.1	7.1	152.6	4.5	105.6	0.0
9 Pup	64096	10.6 ± 6.6	155.5 ± 22.3	14.9	159.2	4.6	77.7	0.0
HR 4523	102365	12.0 ± 6.6	75.9 ± 19.4	7.4	69.6	5.1	85.1	0.0
β Vir	102870	2.9 ± 4.2	31.3 ± 38.2	2.8	81.3	4.4	11.4	1.2
GJ 501.2	114613	37.7 ± 7.7	62.3 ± 5.9	21.7	63.8	16.0	60.3	14.1
i Cen	119756	26.0 ± 7.4	65.2 ± 8.4	19.7	59.8	7.7	79.7	2.1
16 Lib	132052	8.7 ± 6.9	1.2 ± 27.5	7.0	28.2	7.3	155.6	2.3
λ Ser	141004	12.9 ± 8.7	42.0 ± 23.9	3.2	30.5	10.0	45.5	5.1
GJ 667	156384	5.4 ± 7.6	172.2 ± 37.5	5.5	152.8	3.6	27.7	0.0
ψ Cap	197692	18.5 ± 7.8	112.8 ± 14.1	11.9	137.2	13.9	92.8	11.5
ϵ Ind	209100	8.7 ± 8.9	149.0 ± 32.4	2.9	97.7	9.7	157.4	4.0
							Mean $\hat{p}_\star$:	2.9 ± 1.9
Inactive debris disc systems								
ζ Tuc	1581	15.8 ± 6.8	67.0 ± 14.3	6.9	107.3	16.2	54.6	14.7
τ Cet	10700	1.4 ± 3.0	7.0 ± 42.8	2.9	84.8	4.2	178.7	2.9
e Eri	20794	5.2 ± 6.7	31.6 ± 36.2	4.8	46.8	2.6	177.9	0.0
ζ^2 Ret	20807	9.1 ± 8.2	12.7 ± 30.1	9.6	97.0	18.6	9.8	16.7
η Cru	105211	20.7 ± 6.3	72.7 ± 9.0	20.2	82.8	7.6	34.2	4.2
η Crv	109085	11.0 ± 7.9	57.7 ± 25.3	4.8	64.9	6.5	52.5	0.0
61 Vir	115617	3.3 ± 7.2	114.0 ± 42.6	2.2	60.5	4.5	128.2	0.0
HD 207129	207129	28.6 ± 8.0	96.3 ± 8.3	14.1	126.6	24.9	81.6	23.6
							Mean $\hat{p}_\star$:	7.8 ± 2.9
Active stars								
p Eri B	13061	42.2 ± 7.5	135.3 ± 5.1	6.3	90.9	42.5	139.6	41.9
ϵ Eri[c]	22049	30.8 ± 5.7	168.5 ± 5.3	2.6	130.3	30.3	170.9	29.8
o^2 Eri	26965	19.9 ± 6.0	141.6 ± 9.0	4.0	128.5	16.4	144.6	15.2
Procyon	61421	7.5 ± 1.5	154.5 ± 5.8	2.8	158.4	4.7	152.2	4.5
ξ Boo	131156	45.9 ± 5.2	1.9 ± 3.2	1.7	22.5	44.6	1.1	44.3
HD 131977	131977	23.8 ± 8.1	39.3 ± 10.8	1.5	40.5	21.7	39.2	20.1
V2213 Oph	154417	20.1 ± 8.4	39.7 ± 13.8	21.7	35.5	3.4	96.7	0.0
70 Oph	165341	33.8 ± 9.1	105.4 ± 7.9	4.1	31.4	37.3	107.1	36.2
HD 191408	191408	25.6 ± 8.9	117.0 ± 10.7	4.8	132.4	21.6	113.7	19.7
GJ 785	192310	18.7 ± 6.9	85.5 ± 11.6	7.1	130.5	20.0	75.1	18.8
							Mean $\hat{p}_\star$:	23.0 ± 2.2

Notes. [a]Polarization, p, values are given in ppm; angle, θ, in degrees (°); columns 3 and 4 are the same as in Table 4, i subscripts denote interstellar, whilst a star ($\star$) subscript denotes intrinsic polarization.
[b]A manual correction was made to the polarization angle determined for τ^6 Eri. See the text for details.
[c]ϵ Eri also hosts a circumstellar debris disc.

The mean PA method failed in an obvious way for one star out of the 32 in the survey. The polarization angle of τ^6 Eri can be seen in Fig. 6(a) (τ^6 Eri is marked as a cyan point) along with the nearby control stars. It appears that τ^6 Eri lies to just one side of an inflection in the interstellar magnetic field, where the field lines run in near-perpendicular directions; its polarization angle matching the stars at higher declinations very well. Our model used the four nearest stars to determine a polarization angle of 26°.5, where more weight was given to the two stars on the other side of the inflection at lower declinations, the result can be seen in Fig. 6(b). To compensate, we have excluded the two control stars at lower declinations from the determination, and used only the other two to produce a polarization angle of 134°.1, which is very close to matching τ^6 Eri's measured polarization angle of 132°.8.

The results of the interstellar subtraction are given in Table 8. The magnitude of polarization of the active stars is shown to be 10 times greater than inactive non-debris disc stars. And, in contrast to the pre-interstellar subtraction result given in Table 5, the debris disc stars have a magnitude of polarization 1σ higher than the inactive non-debris disc stars. Not shown are the break-downs for binaries or exoplanet hosts, neither of which are significantly different to single stars or non-exoplanet hosts, respectively, after interstellar subtraction. In Fig. 7, we plot the calculated intrinsic polarizations on an H–R diagram. This serves to demonstrate that there is little intrinsic polarization to be found in F- and G-type main-sequence stars, and emphasize the polarization seen in the later type active stars.

4.4 Ordinary FGK dwarfs

The ordinary FGK dwarfs were included in our determinations of $\hat{p}/d$ in Section 4.2.1, which were subsequently used in the interstellar subtraction in Section 4.3. However, this should not be a significant impediment to identifying trends within this group of

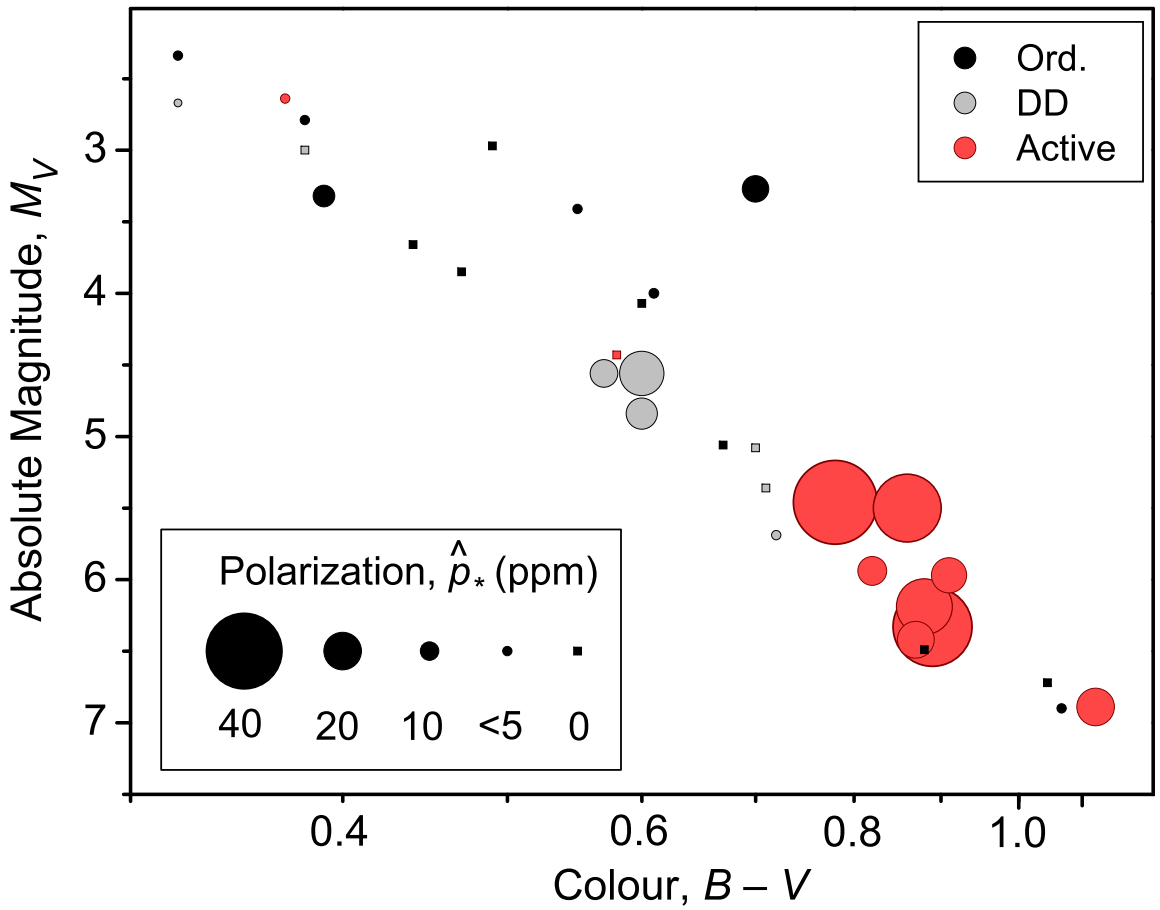

Figure 7. H–R diagram showing the debiased intrinsic polarization for the FGK dwarfs of our survey. It is clear that active stars are more highly polarized, particularly those of $B-V$ colour greater than 0.75. A few debris disc systems can also be seen to have elevated polarization magnitudes. For most ordinary FGK dwarfs, we calculate no significant intrinsic polarization.

stars because the polarization angle associated with intrinsic polarization will be randomly distributed with respect to the polarization angle of interstellar polarization. Whilst the mean value of $\hat{p}/d$ can be expected to be elevated from its true value if intrinsically polarized stars are included, if $p_\star \sim <p_i>$, the effect will be small and intrinsically polarized stars will still show up as a result of differences in angle.

4.4.1 Outliers

In Fig. 8, we have plotted $\hat{p}_\star$ against distance for the ordinary FGK dwarfs. There is no evident trend, indicating that our interstellar subtraction is doing a reasonably good job. However, in Figs 7 and 8, and in Table 8, there are two stars that stand out with a calculated intrinsic polarization significant at around the 2σ level; those being the G3 dwarf GJ 501.2 and the F5 dwarf ψ Cap, at distances of 20.7 and 14.7 pc, respectively.

Seeking an explanation for the polarization of ψ Cap, we note that it does not have a significant infrared excess (Moro-Martín et al. 2015), and Lagrange et al. (2009) has ruled out planets with a minimum mass of $m \sin i$ of 0.4 $M_{\rm Jup}$ with orbital periods less than 3 d. The possibility that the polarization is a result of it being an unidentified active star is made unlikely due to its $B-V$ colour of 0.39 (refer to 4.6). However, it is interesting to note that ψ Cap was the first star shown to have differential rotation using line-profile

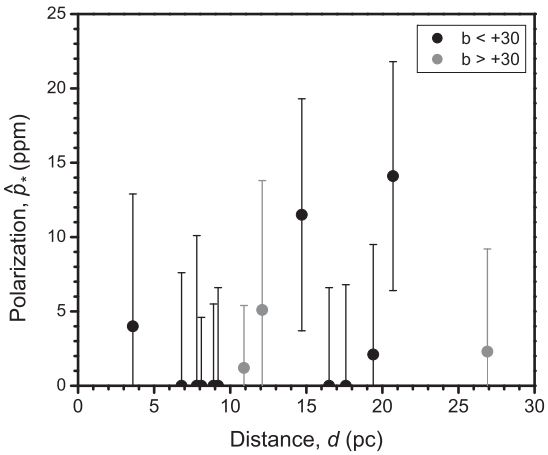

Figure 8. Intrinsic polarization plotted against distance for ordinary FGK dwarfs.

analysis and that its rotation rate is roughly 20 times that of the Sun (Reiners, Schmitt & Kürster 2001).

GJ 501.2 is an old (8 Gyr) and inactive star according to references within Sierchio et al. (2014), so we do not expect activity to be the cause of the calculated intrinsic polarization. It may have an infrared excess at 70 μm (Sierchio et al. 2014), having made a detection a little below the significance they consider reliable. If

correct $L_{\rm dust}/L_\star \sim 10 \times 10^{-6}$, which, under ordinary circumstances, is enough to account for up to (but probably less than) 5 ppm of the polarization signal. GJ 501.2 is also an exoplanet host system (Wittenmyer et al. 2014), where the planet has an orbital period of 10.5 yr, and a minimum mass $m \sin i$ of 0.48 $M_{\rm Jup}$, which is not remotely large or close enough to expect any significant polarization signal from Rayleigh scattering (Seager et al. 2000). The current radial velocity limits for the system rule out planets with greater than 8 $M_{\rm Earth}$ in orbits with semimajor axis, $a < 0.05$ au at 99 per cent confidence (Wittenmyer, private communication).

The most likely explanation for the *calculated* intrinsic polarization for both stars is probably interstellar polarization coupled with measurement uncertainty. Both GJ 501.2 and ψ Cap are in the dustier $b < +30$ region and at a distance where the uncertainty in $\hat{p}/d$ is greater – the 15–25 pc distance identified as having an elevated $\hat{p}/d$ in Fig. 2. In the case of GJ 501.2, the case is particularly strong for a dustier ISM; as, from Table 8, it can be seen that the calculated angle of interstellar polarization very closely matches the measured angle of polarization. The case is not as strong for ψ Cap, but it still seems the most likely explanation.

4.4.2 *Binaries and exoplanet hosts*

Five ordinary FGK dwarfs are in multiple systems: HR 4523, 9 Pup, i Cen, GJ 667 and p Eri A. GJ 501.2, GJ 667 and HR 4523 also host exoplanets. Other than GJ 501.2, only the spectroscopic binary i Cen exhibits intrinsic polarization at any level of significance, and with a debiased polarization of only 2.1 ppm, this is not worth speculating on further.[5] These null results come despite the fact that the B components of GJ 667, i Cen and 9 Pup are inside the HIPPI aperture. Young close binaries sometimes exhibit intrinsic polarization due to gas that is entrained between the stars (McLean 1980) or in the outer atmosphere of one of them (Clarke 2010). Such a mechanism was invoked to try and explain the variable polarization of the young (∼70 Myr) solar type star HD 129333 Elias & Dorren (1990). Our data suggest that this phenomena is not present in any of the stars studied here.

4.4.3 *FGK stars in general*

From Table 8, there is very little, if any, intrinsic polarization in the ordinary FGK dwarfs, and no trends in $B - V$ colour or spectral type are evident. The best explanation for any *calculated* intrinsic polarization here is patchiness in the dust density of the ISM in combination with statistical noise from the measurements. We therefore conclude that any increase in polarization seen in later spectral classes, such as that suspected by Tinbergen & Zwaan (1981) and Tinbergen (1982) must be restricted to active stars, or higher luminosity classes as identified by Cotton et al. (2016a), or restricted to other wavelengths outside the g' band. This means that in the g' filter, inactive FGK dwarfs that do not host debris discs are good probes of the local ISM, and as such make suitable interstellar calibrators for other interesting objects.

[5] ϵ Ind has a candidate planetary companion, and a debiased polarization of 4.0 ppm, but the planetary candidate is much too far from the star, and if the polarization measured is anything other than statistical noise, then a very low level of stellar activity (Zechmeister et al. 2013) is more likely to be responsible.

4.5 Debris disc stars

In Table 8, there are three debris disc stars with a debiased polarization of zero, one with a marginal detection – HD 207129 – and two with signals above the 2σ level. Among the factors that can influence the polarization seen from a debris disc system is its geometry with respect to the aperture. If a disc is contained wholly within the aperture, then we expect the polarization vector to be aligned perpendicular to the long axis of its elliptical projection on the sky. If, on the other hand, only the edges of a system inclined edge-on are within the aperture, the opposite might occur. A face-on system should be substantially unpolarized, so long as it is centred in the aperture. In order to try to make sense of this mixed bag of marginal- and non-detections, we have plotted the basic system geometry of each disc system in comparison with our aperture, along with the measured polarization in Fig. 9. We have also tabulated the system parameters in Table 9 for reference.

Dealing with the non-detections first, e Eri (HD 20794) is the only system contained wholly within the HIPPI aperture, but it has a fractional luminosity, $L_{\rm dust}/L_\star$, of 2.4×10^{-6}, which, in optimistic circumstances, would not be expected to produce a fractional polarization signal of more than 1.2 ppm. The case of 61 Vir (HD 115617) is more interesting; most of the disc is in the aperture, and it has an $L_{\rm dust}/L_\star$ of 27.6×10^{-6}. Modelling of the disc inferred an albedo of <0.31, dominated by 1 μm grains (Wyatt et al. 2012). The non-detection of polarization from this system (4.5 ± 7.2 ppm) is consistent with their analysis, wherein we would expect a fractional polarization at the level of ≤9 ppm from the whole disc. A more complex case is that of η Crv (HD109085); it has a two-component debris disc, with the inner, warm component likely delivered by bodies scattered inward from the outer disc (Duchêne et al. 2014). The outer, cold component lies outside the HIPPI aperture, but the warm component of the disc is relatively bright, $L_{\rm dust}/L_\star$ of 325×10^{-6}, and lies well within the HIPPI aperture at separations down to 1 au from the star (Defrère et al. 2015). In this case, we might infer that the dust is smoothly distributed within the HIPPI aperture, resulting in a non-detection of polarization from the system.

We record for τ Cet (HD 10700) a very low polarization, significant only at the 1σ level. However, it only has an $L_{\rm dust}/L_\star$ of 7.8×10^{-6} and marginally resolved Herschel observations suggest a broad, smooth disc (Lawler et al. 2014), so we wouldn not expect to see more polarization than is detected even with the most favourable system geometry and grain properties. Most of the τ Cet disc is contained within the aperture, and the polarization vector is roughly perpendicular to the position angle of the disc, which is what might be expected.

The η Cru (HD 105211) system has a large infrared excess but it falls mostly outside the HIPPI aperture. The system as plotted may be misleading in this case, as the η Cru disc shows signs of asymmetry (Hengst et al. 2017). However, the parts of the disc that lie within the aperture are the edges (as opposed to the ends) of the elliptical projection. The orientation of the polarization vector is consistent with what we might expect in this case.

An interesting case is ζ^2 Ret (HD 20807). It is the system that initially stood out in Fig. 1; most of its disc lies within HIPPI's aperture, but its infrared excess is not at all large, only 10.0×10^{-6}. Although our detection is formally only 2.3σ, a polarization of ∼17 ppm is implied. The debris disc in this system is believed to be highly asymmetric (Eiroa et al. 2013; Faramaz et al. 2014). Our measurement here supports that finding. We have previously seen that asymmetry within a debris disc system can produce a larger polarization than would otherwise be expected. In our work on ϵ Sgr

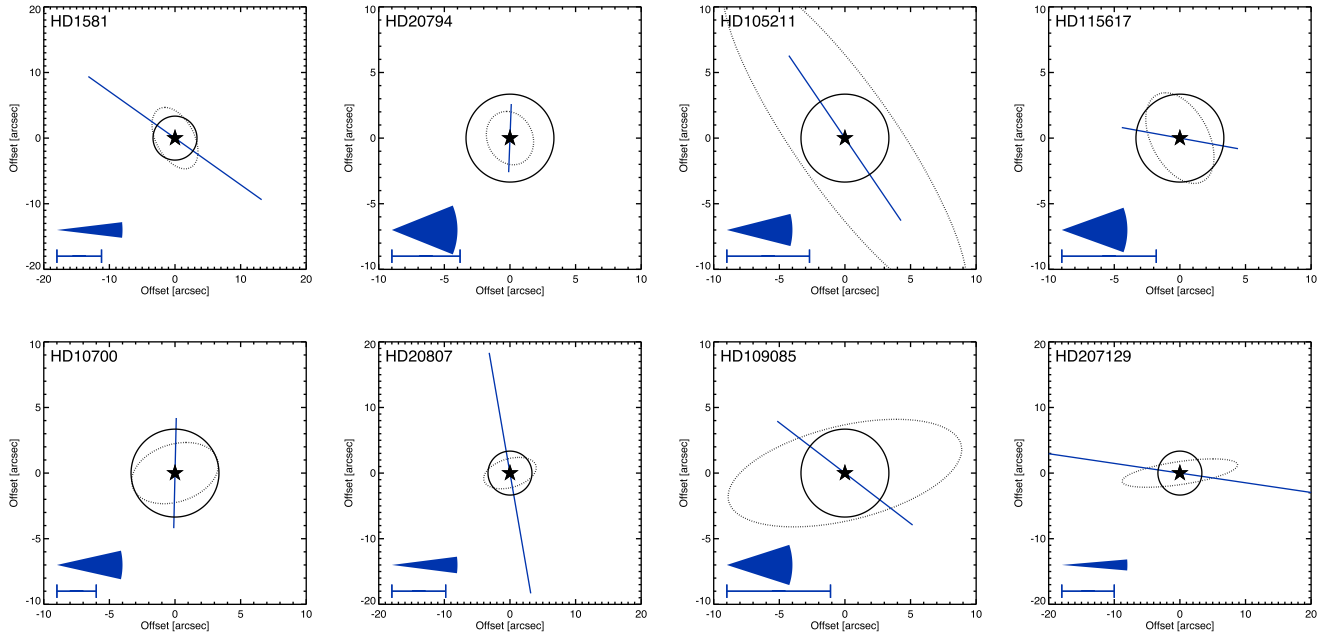

Figure 9. A comparison of characteristic debris disc system parameters with the HIPPI aperture, along with polarization vectors. The dotted line shows the geometry of the disc at its characteristic radius. The solid black line shows the HIPPI aperture centred on the star. The solid blue line centred on the star shows the magnitude and angle of the polarization measured for the system (the scale marked on the individual plots also applies to the polarization vectors). The size of the 1σ error in polarization magnitude is shown in the bottom left hand corner of the plots by the capped blue bar, and the 1σ error in the angle corresponds to the angle of the blue wedges, also in the bottom left hand corner of each plot.

Table 9. Debris disc properties.

Name	HD	$r^a_{\rm disc}$ (arcsec)	$i^b_{\rm disc}$ (°)	$\theta^b_{\rm disc}$ (°)	$L_{\rm dust}/L^a_\star$ (10^{-6})
ζ Tuc	1581	3.5	21	64	16.0
τ Cet	10700	3.3	35	105	7.8
e Eri	20794	1.8	50	8	2.4
ζ^2 Ret	20807	4.0	65	110	10.0
η Cru	105211	9.3	55	30	74.0
η Crv	109085	8.9	47	116	21.7
61 Vir	115617	2.6	20	65	27.6
HD 207129	207129	8.8	60	120	83.0

Notes. [a]The debris disc characteristic radius ($r_{\rm disc}$ converted from astronomical units) and fractional infrared excess ($L_{\rm dust}/L_\star$), have been taken from the following references: ζ Tuc (Trilling et al. 2008; Montesinos et al. 2016), τ Cet (Lawler et al. 2014), e Eri (Marshall et al. 2014), ζ^2 Ret (Eiroa et al. 2013), η Cru (Hengst et al. 2017), η Crv (Duchêne et al. 2014), 61 Vir (Wyatt et al. 2012) and HD 207129 (Marshall et al. 2011).
[b]The debris disc inclination ($i_{\rm disc}$) and position angle ($\theta_{\rm disc}$) have been taken from the following references: ζ Tuc (Montesinos et al. 2016), τ Cet (Lawler et al. 2014), e Eri (Kennedy et al. 2015), ζ^2 Ret (Eiroa et al. 2010), η Cru (Hengst et al. 2017), η Crv (Duchêne et al. 2014), 61 Vir (Wyatt et al. 2012) and HD 207129 (Marshall et al. 2011; Löhne et al. 2012).

(Cotton et al. 2016c), we demonstrated that a secondary component illuminating part of the disc could produce a large polarization. The polarigenic effect of a disc that has a significantly uneven dust distribution would be similar. The wide binary companion, ζ^1 Ret, is separated from ζ^2 Ret by 309 arcsec, has a similar spectral type and no infrared excess; measurements of it would provide a very precise interstellar calibration, enabling confirmation of the polarization signal calculated here.

Another system with a 2σ detection and polarization greater than its infrared excess would suggest is ζ Tuc (HD 1581). In this case, the alignment of the polarization vector is not easily explainable by the system geometry. We can probably rule out an extra unsubtracted intrinsic component as the cause here because the star is quite close, only 8.6 pc. The aperture and the disc are similar sizes, so if the aperture has been positioned too far off-centre, we could have artificially created an asymmetry leading to a detectable polarization signal, but we do not have any reason to believe this is the case. If real, our measurement indicate some asymmetry in this disc system as well.

HD 207129 is the only debris disc system for which we have a 3σ detection. It is a system that is fairly edge on ($i_{\rm disc} = 60°$), where the HIPPI aperture has observed the edges of the elliptical projection, but not the ends. HD 207129's infrared excess is the largest of the objects we tabulated in Table 9, so we expected a detectable polarization with a vector parallel to the position angle of the debris disc. Fig. 9 shows that this is close to being the case. The polarization vector is inclined $\sim 18°$ from alignment, with the 1σ error on our polarization angle determination being $9\overset{\circ}{.}7$. The polarization signal is $\sim$30 per cent of the infrared excess, which is interesting in light of the disc's faint emission in scattered light (implying a low albedo; Krist et al. 2010) and inferred large minimum dust grain size (Löhne et al. 2012).

4.5.1 Hot dust stars

In addition to hosting a debris discs, τ Cet and e Eri are both hot dust stars (di Folco et al. 2007; Ertel et al. 2014). Hot dust is the name given to the phenomena of significant infrared excesses at near-infrared wavelengths (Absil et al. 2013; Ertel et al. 2014). The origin of the hot dust signal is still a mystery, with a leading theory being nanoscale grains (Su et al. 2013; Rieke, Gáspár & Ballering 2016). Recently, Marshall et al. (2016) placed a strict upper limit on the polarimetric signal due to hot dust of 76 ppm in the g' band, but with a possible signal of $\sim$17 ppm. Intriguingly, Ertel et al. (2016)

have recently published data suggesting the phenomenon may be variable.

We measure no significant polarization for e Eri – it is one of the least polarized objects in the survey. Either the hot dust produces no polarization in this system or there was no hot dust present at the time of the observation.

We have two observations of τ Cet, which, when averaged, give the small polarization reported in Table 8. If, on the other hand, we do not interpret the data as statistical scatter in the measurements but real variation, and do the intrinsic subtraction on each observation separately, we get values of $p_\star = 7.9 \pm 4.1$ ppm, $\theta_\star = 47\overset{\circ}{.}9 \pm 18.5$ on 2015/06/26 and $p_\star = 11.2 \pm 4.3$ ppm, $\theta_\star = 148\overset{\circ}{.}4 \pm 13\overset{\circ}{.}0$, four months later on 2015/10/20. Particular caution needs to be taken here in interpreting these results as being due to intrinsic variability. To begin with, they are hardly significant, but it needs to be said that these measurements have different TP calibrations, and at these levels, small differences in the calibration will bias results in favour of variability. Nevertheless, the difference is not inconsistent with the possible signal level of ∼17 ppm inferred by Marshall et al. (2016). We recommend long-term polarimetric monitoring of stars with significant hot dust signatures.

4.6 Active stars

We report here for the first time unambiguous detections of linear broad-band polarization in active FGK dwarfs using an aperture technique. The stars p Eri B, ϵ Eri, ξ Boo and 70 Oph all record calculated intrinsic polarizations well in excess of 3σ. For ξ Boo, the signal is more than 8σ. Additionally, every active star in the survey except V2213 Oph records a greater than 2σ detection after interstellar subtraction. In contrast, the only inactive star in the survey with a calculated intrinsic polarization greater than 3σ is the debris disc system HD 207129. Indeed the interstellar subtraction was hardly necessary to establish polarization in the active stars, all but one is within 10 pc and the difference between active and inactive stars was already clear in Table 5.

4.6.1 Multiple observations of Procyon

Procyon also records a 3σ signal, but we are not as confident in this detection. The reported measurement is the error-weighted mean of three observations, including one in 2015 October. The polarigenic mechanisms expected for active FGK dwarfs imply variable polarization. Because polarization is a pseudo-vector, averaging the Stokes parameters q and u from multiple measurements will underestimate the true magnitude of intrinsic polarization if it is variable. In this case, an alternative formulation can be used, where each individual measurement is debiased (after interstellar subtraction) and the mean of the individual $\hat{p}_\star$ measurements is taken. If one does this for Procyon, one gets 6.3 ± 1.5 ppm, which is still at the 3σ level, but slightly less than the result reported in Table 8, and makes it more likely, given the small magnitude of polarization, that statistical noise or small inconsistencies in the TP calibration between 2015 and 2016 could be responsible for the detection in this case.

4.6.2 The potential influence of ϵ Eri's derbis disc

ϵ Eri is both an active star and a debris disc system. Potentially, there are components of polarization due to both of those properties. As a group, the systems covered in Section 4.5 are not nearly as polarized as the active stars. We would therefore expect

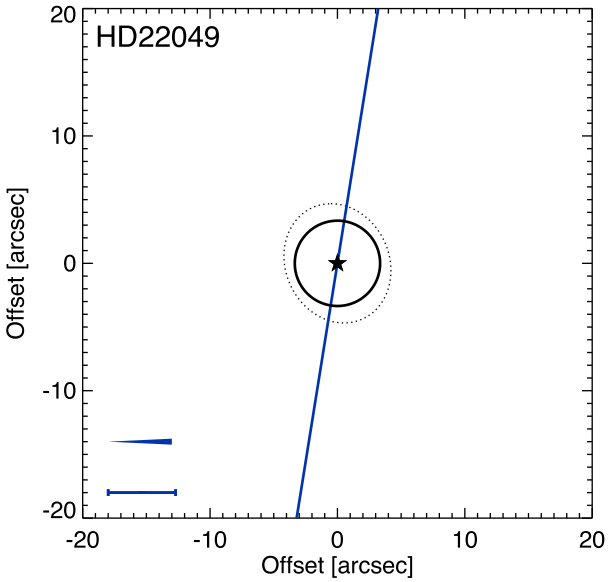

Figure 10. A plot of the polarization and system geometry of ϵ Eri. The diagram is laid out as per Fig. 9, i.e. the dotted line shows the geometry of the inner belt at the outer radius of the unresolved emission shown in Chavez-Dagostino et al. (2016). The solid black line shows the HIPPI aperture centred on the star. The solid blue line centred on the star shows the magnitude and angle of the polarization measured for the system (the scale marked on the individual plots also applies to the polarization vectors). The size of the 1σ error in polarization magnitude is shown in the bottom left hand corner of the plots by the capped blue bar, and the 1σ error in the angle corresponds to the angle of the blue wedges, also in the bottom left hand corner of each plot. The system parameters come from Marshall et al. (2014), Greaves et al. (2014) and Chavez-Dagostino et al. (2016): $r_{\rm disc} = 4.2$ arcsec, $i_{\rm disc} = 32^\circ$, $\theta_{\rm disc} = 7^\circ$.

that ϵ Eri's activity is the dominant component. However, it does have a larger total infrared excess than any of the other systems: $L_{\rm dust}/L_\star = 107.6 \times 10^{-6}$. The excess is mainly due to the outer cold component, the inner warm belt around 3 au has an excess of 33×10^{-6} (Backman et al. 2009). We have plotted the system's parameters (for the inner belt) and polarization as we did for the other debris disc systems in Fig. 10. It can be seen that the characteristic radius of the belt falls just outside the HIPPI aperture. The inner system is potentially awash with dust, and no distinction can currently be made between broad or narrow architectures for the debris belts in the inner part of the system (Chavez-Dagostino et al. 2016). The disc thus possesses an inner component that falls within the HIPPI aperture. Perhaps most importantly, the disc/belt has a near face-on inclination. As a result, we would expect little contribution to the polarization due to the symmetry within the aperture. We therefore attribute the polarization seen to the star's activity.

4.6.3 Scattering mechanisms

Recently, Kostogryz & Berdyugina (2015) have made calculations of limb polarization to expect in FGK dwarfs and then used this result (Kostogryz, Berdyugina & Yakobchuk 2015) to determine the limb polarization to expect from selected (exoplanet host) FGK dwarfs due to much smaller star spots; the result being ∼2–3 ppm for a spot covering 1 per cent of the stellar disc. For this mechanism to explain our results, spot filling factors would have to far exceed that level. Some time prior to this, Saar & Huovelin (1993) tabulated the results of models estimating the maximum magnitude of limb polarization from Thompson and Rayleigh scattering that might be

caused by stellar activity. Thompson scattering could not explain the magnitude of polarization we see here.

Rayleigh scattering under optimal conditions can explain or come close to explaining our measurements. Spot sizes with filling factors of around 18 per cent optimally positioned on the surface (which represent the conditions for maximum polarization) could produce some of the levels of polarization we see. Kostogryz & Berdyugina (2015)'s models indicate that linear polarization falls off quite rapidly away from the stellar limb, so Saar & Huovelin (1993)'s tabulated values represent the rare best-case scenarios. However, in low-mass active stars, the required level of spot coverage is possible (Jackson & Jeffries 2013). Saar & Huovelin (1993)'s specific calculations for Procyon and ϵ Eri produce 5 and 33 ppm in B band under these conditions, respectively; in g', their plots imply that it should be about two-thirds of that, which is a little less than we measured, and a fair bit less than Kochukhov et al. (2011) found from spectropolarimetric measurement of ϵ Eri. The equivalent figure for ξ Boo in g' band is $\sim$100 ppm. Toner & Gray (1988) have developed a model for ξ Boo based on spectroscopic observations that gives filling factors of 10 ± 5 per cent for a feature at a latitude of $55^\circ \pm 8^\circ$. So, our measurement fits the prediction for Rayleigh scattering in this instance.

However, the geometrical requirements for a Rayleigh scattering solution makes this mechanism seem less likely, since multiple spots sub-optimally positioned will have their effects begin to cancel out. ξ Boo has a rotation period of 6.43 ± 0.01 d (Toner & Gray 1988). We made two measurements of it exactly 3 d apart. Those measurements are not significantly different, but a change in $\theta_\star$ of only $\sim 5^\circ$ is implied. If the polarization is to be attributed to a single starspot (or single patch of spots), this should not be the case unless we assume that the most contrived possible combination of timing and geometry or the star was rotating pole-on – which is not consistent with determining a rotation period from photometry.

4.6.4 *Magnetic fields*

A more likely polarigenic mechanism for late dwarfs is differential saturation. Active FGK dwarfs manifest net global fields of several to tens of Gauss (Marsden et al. 2014). Through the Zeeman effect, these fields manifest as circular polarization that is readily detected with spectropolarimetry (Fares et al. 2010; Morgenthaler et al. 2012; Jeffers et al. 2014). Weaker linear polarization will result from the same processes (Donati & Landstreet 2009). Because it is weaker, and the line profiles more difficult to model, only recently have Kochukhov et al. (2011) managed to detect linear polarization in an FGK dwarf using spectropolarimetry. At present, there are no model predictions for broad-band polarization based on the global fields of active FGK dwarfs. There are, however, older models for the broad-band polarization to expect from the && kG fields associated with starspots (Landi Degl'Innocenti 1982; Leroy 1990; Huovelin & Saar 1991; Saar & Huovelin 1993; Stift 1997).

Saar & Huovelin (1993)'s models produce roughly an order of magnitude greater polarization for differential saturation than Rayleigh scattering for the same spot size that, if one considers an uneven distribution of spots, matches better with what we see here. If we were to interpret our results in terms of the starspot models of Huovelin & Saar (1991) and Saar & Huovelin (1993), the polarization magnitudes suggest spots with filling factors of $\sim$0.25 per cent for the less active stars to 2.0 per cent for ξ Boo. However, present mapping work using circular polarization points to significant cancellation of small-scale structure by features of opposite polarity. In light of this shift in understanding since the models were developed, their quantitative predictions are unlikely to be instructive.

Qualitatively, there are two predictions of differential saturation testable with our data. The first is that polarization increases for later stellar types (in the temperature range 4000–7000 K) (Saar & Huovelin 1993) (or with $B - V$ colour; Patel et al. 2016). This comes about because of the increased line-blanketing in later types. The behaviour is complicated because lines are not evenly distributed, and with oversaturation, net polarization is reduced. The second prediction is that more active stars – those with stronger magnetic fields and/or greater degrees of micro-turbulence – have enhanced Zeeman splitting that increases polarization (Stift 1997; Patel et al. 2016). These predictions are complicated by considerations of geometry (Tinbergen & Zwaan 1981; Huovelin & Saar 1991) and wavelength dependence (Saar & Huovelin 1993; Patel et al. 2016). The geometrical considerations are the most difficult to parse given a modern view of magnetic field structure in these stars, and we have neglected it here. Regarding wavelength dependence, Saar & Huovelin (1993) made specific calculations for standard Johnson bands, whereas our measurements are made in the SDSS g' band that has an effective wavelength between the B and V bands. Their trends are similar for the B and V bands though, with the V-band polarization predicted to be roughly two-fifths to one quarter of that in the B band, depending on the stellar parameters.

To test the qualitative predictions of Saar & Huovelin (1993)'s models, in Fig. 11, we have plotted the debiased intrinsic polarization of each active star against the activity indicator $\log(R'_{HK})$ and the photometric colour $(B - V)$.[6] These data are also tabulated in Table 10. It should be noted that the literature values for $\log(R'_{HK})$ come predominantly from Martínez-Arnáiz et al. (2010). Using a single literature source ensures consistency, but activity levels vary over time, and these measurements were more than 5 yr old at the time of our observations. Bearing in mind this caveat, and those stated above, there is some support for the differential saturation models in the data. The two least polarized active stars, Procyon and V2213 Oph, are also the two with the lowest $B - V$ colour values. This is despite them being nominally more active.

There are seven active dwarfs with $B - V$ values between 0.75 and 0.90. Of those, two of the three least polarized have the lowest (most negative) activity indices. The third is GJ 785, for which our $\log(R'_{HK})$ value comes from Jenkins et al. (2006). However, GJ 785 was also observed by Martínez-Arnáiz et al. (2010), who classified it as not active. So, it should probably be much lower on the diagram. This then supports the notion that for a given temperature, less active stars are less polarized.

If the same global fields measured by spectropolarimetry with circular polarization are responsible for the broad-band linear polarization we measure, then we should see a correspondence between the net field and our measurements. To test this, we have looked at data for stars we have in common with two spectropolarimetric surveys of magnetic fields, BCool (Marsden et al. 2014) and PolarBase (Petit et al. 2014), and obtained determinations of the net longitudinal magnetic field (B_l), using the formulation of (Donati et al. 1997). For stars in the PolarBase database, we downloaded the observations and created Stokes V LSD (Least-Squares Deconvolution; Donati et al. 1997), using the same line masks used by the BCool collaboration (Marsden et al. 2014). To do this, we

[6] For reference, a nominal F0 dwarf has a characteristic temperature of 7200 K and a $B - V$ colour of 0.294; G0 5920 K and 0.588; K0 5280 K and 0.816; and K5 4450 K and 1.134 (Pecaut & Mamajek 2013).

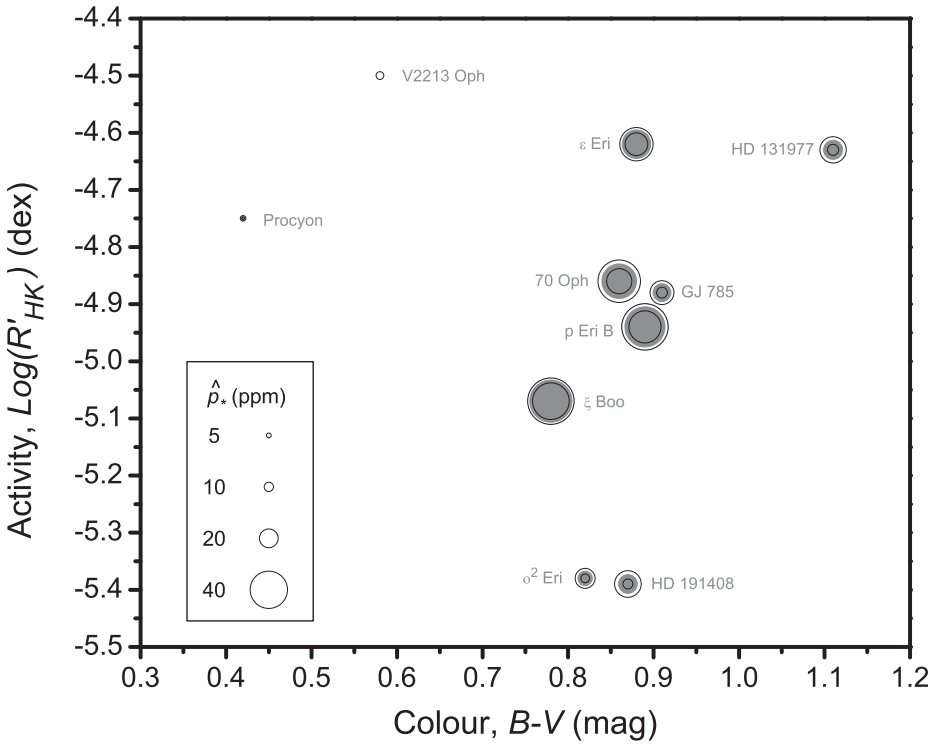

Figure 11. A plot showing the determined intrinsic polarization of active stars in this study relative to their colour and activity index. The areas of the grey circles represent the debiased intrinsic polarization, whilst the solid circles are the 1σ errors.

Table 10. Selected properties of active stars.

Name	HD	$B-V$	Abs mag (V)	Activity[a] $\log(R'_{HK})$
p Eri B	10361	0.89	6.33	−4.94
ϵ Eri	22049	0.88	6.19	−4.62
o^2 Eri	26965	0.82	5.94	−5.38
Procyon	61421	0.42	2.64	−4.75
ξ Boo	131156	0.78	5.46	−5.07
HD 131977	131977	1.11	6.89	−4.63
V2213 Oph	154417	0.58	4.43	−4.50
70 Oph	165341	0.86	5.50	−4.86
HD 191408	191408	0.87[b]	6.42	−5.39
GJ 785	192310	0.91	5.97	−4.88

Notes. [a]The activity index comes from Martínez-Arnáiz et al. (2010) for all stars listed except for GJ 785 that is the mean of two values reported by Jenkins et al. (2006), and Procyon for which we have taken the S-index value form Hempelmann et al. (2016) and converted it to $\log(R'_{HK})$ using the relations for dwarf stars of Middelkoop (1982) and Noyes, Weiss & Vaughan (1984) as related by Schröder, Reiners & Schmitt (2009). Further, it should be noted that Noyes et al. (1984)'s relation is strictly only valid for $B-V>0.44$, and that Procyon falls just outside this range (0.42), so the $\log(R'_{HK})$ value obtained is not as reliable as for the other stars listed.
[b]SIMBAD $B-V$ is unreliable for this star; we have substituted data from Martínez-Arnáiz et al. (2010).

Table 11. Longitudinal magnetic field measurements from BCool and PolarBase.

Name	HD	$B-V$	Obs.	Ref.[a]	$\lvert B_l\rvert$ (G) max	min
Active stars						
ϵ Eri	22049	0.88	58	B	-10.9 ± 0.2	$+0.4\pm0.2$
o^2 Eri	26965	0.82	1	B	$+1.3\pm0.2$	
Procyon	61421	0.37	1	P	$+2.0\pm0.7$	
ξ Boo[b]	131156	0.78	101	B	$+18.4\pm0.3$	$+0.5\pm1.0$
GJ 785	192310	0.91	1	P	-3.9 ± 0.2	
Inactive stars						
τ Cet	10700	0.57	2	P	-1.8 ± 0.9	$+1.2\pm0.8$
π^3 Ori	30652	0.45	5	B,P	-4.9 ± 1.7	$+1.3\pm0.7$
γ Lep	38393	0.47	6	P	-3.3 ± 1.3	-0.4 ± 0.4
β Vir	102870	0.55	3	P	$+3.3\pm0.9$	-0.9 ± 0.1
61 Vir	115617	0.70	1	P	-0.2 ± 0.2	

Notes. [a]P: PolarBase (Petit et al. 2014), B: BCool (Marsden et al. 2014).
[b]The data presented are for HD 131156A; $\lvert B_l\rvert_{\max}$ for HD 131156B is similar.

assumed a stellar temperature for each star based on information in the PASTEL database (Soubiran et al. 2016). The velocity range over which B_l is calculated has been chosen to maximize $|B_l|/\Delta B_l$ as in the BCool work (Marsden et al. 2014). We have tabulated minimum and maximum B_l values obtained for stars we have classified as both active and inactive in Table 11.

From Table 11, there are many observations of ϵ Eri and ξ Boo, and we can be confident that the strength of the field is captured by the observations. For a further three of the active stars, there is only a single observation. The configuration of the magnetic field can vary substantially over/within a rotation period and an activity cycle – large regions of positive and negative field can cancel each other out – and as a result, it is difficult to know if these measurements are representative. Similarly, we have a handful of observations for a further five stars we have classified as inactive.

We have plotted $\hat{p}_\star$ against the greatest field recorded for each star ($\lvert B_l\rvert_{\max}$) in Fig. 12. With the caveat that the data are sparse, the stars

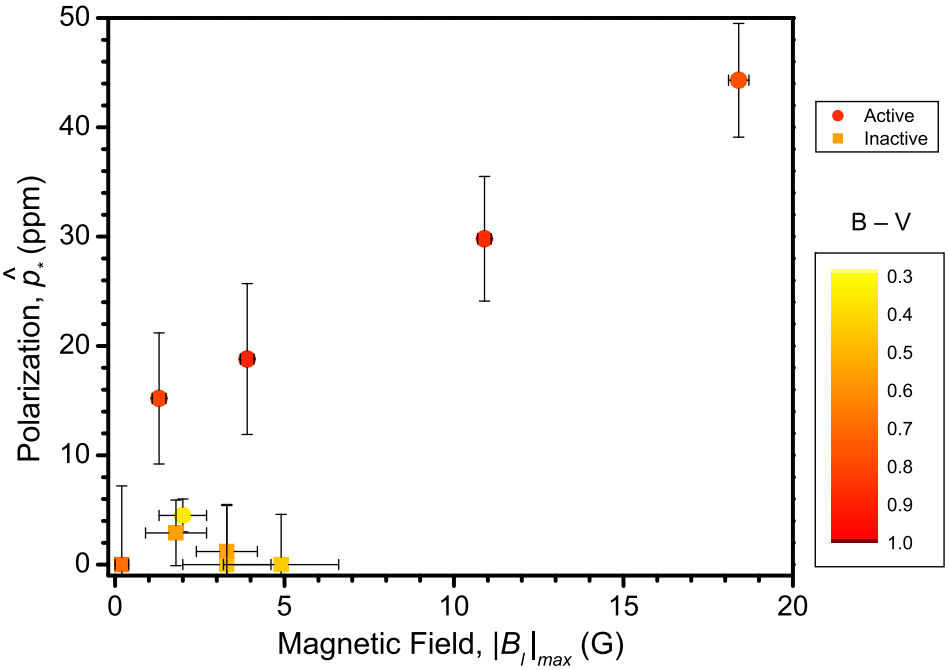

Figure 12. A plot showing the determined intrinsic polarization of active stars in this study relative to their maximal longitudinal magnetic field determined from spectropolarimetric circular polarization measurements. The colour scale denotes the $B - V$ colour of the stars. Stars we classified as active in this study are denoted by circles, inactive stars by squares.

with the strongest longitudinal magnetic fields also recorded the greatest linear polarization. Although the stars with $|B_l|_{max}$ less than 5 G have fewer observations, of those, the cooler stars ($B - V > 0.75$) measured greater linear polarizations. This suggests that for cooler stars, which we expect to have greater line-blanketing, the magnetic field strength determined from circular polarization is predictive of linear polarization. Further work will be needed to be done to test this hypothesis, to determine how circular polarization is related to broad-band linear polarization and how they are related over an activity cycle or modulated over a rotation period. It is also desirable to probe cooler objects like M-dwarfs where increased line-blanketing could potentially oversaturate the spectral lines within a band and reduce the measurable polarization. Leroy (1990) concluded that the blending of spectral lines resulted in a limit to the maximum polarization from differential saturation, and that this was already reached in the blue part of the spectrum for solar types. The models of Stift (1997) show polarization increasing with reducing temperature in the visible part of the spectrum, but at a decreasing rate on a per Kelvin basis.

4.6.5 A comparison with previous linear polarization measurements of active dwarfs

At this juncture, it is pertinent to point out that the magnitudes of polarization we record in our data are well below those suggested by other studies of active late dwarfs. Most recently, Patel et al. (2016) reported 800 ± 60 ppm in the *V* band, and 1600 ± 100 ppm in the *B* band. Alekseev (2003) reports even higher levels of polarization than this. Whilst Patel et al. (2016) have observed, on average, more active stars, this seems in extraordinarily poor agreement with our mean in g' of 23.0 ± 2.2 ppm. The most polarized object in the work of Huovelin et al. (1988) is the same object that is most polarized of those we report here – ξ Boo – for it, they report 400 ± 60 ppm in the *V* band, and 340 ± 140 ppm in the *B* band. The intrinsic polarization we calculate in g' for ξ Boo is an order of magnitude less than this. Differential saturation is highly wavelength-dependent, and the models of Saar & Huovelin (1993) clearly indicate that polarization in the *B* band is expected to be a few times that in the g' filter, but they also indicate that the *V*-band polarization will be less than that of g'.

Whilst the contention of Clarke (1991) and Leroy (1989) that Huovelin et al. (1988)'s measurements were affected by scattered moonlight has already been mentioned, Patel et al. (2016)'s results are new and we need to examine why there might be a discrepancy between their results and ours. Their instrument made use of a rotatable half wave plate to provide polarizaiton modulation. Such a set-up is susceptible to scintillation noise due to seeing (see Kemp et al. 1987b; Hough et al. 2006; Wiktorowicz & Matthews 2008; Bailey et al. 2015 and references within), and is not well suited to measuring polarization at the ppm level. This combined with the faintness of the targets they observed (all fainter than $m_V = 6$ due to limitations of their CCD detector) means it is probable that their observations are dominated by noise. It is difficult to know what to make of Alekseev (2003)'s measurements given that he has made use of the same instrument, telescope and statistical techniques as Huovelin et al. (1988) but sees even larger polarizations. It is probable that these are also dominated by scintillation noise. Alekseev (2003) attributed the difference between his measurements and the predictions of Huovelin & Saar (1991) and Saar & Huovelin (1993) to additional circumstellar material; something we do not see evidence for in our results for ordinary FGK dwarfs.

Kochukhov et al. (2011) used the HARPSpol instrument (Piskunov et al. 2011; Snik et al. 2011) installed at the Cassegrain focus of the 3.6 m telescope at the European Southern Observatory to make observations of three stars including ϵ Eri in 2011. HARPSpol is a spectropolarimeter (operating over a wavelength range of 380–690 nm) that makes use of LSD to determine a polarization. Kochukhov et al. (2011) monitored ϵ Eri for the 11 nights of its

rotation period, and report linear polarization determinations from the LSD amplitudes in q and u for the three nights where they have sufficient signal to noise for marginal or definite detections. Their results are reported in terms of individual Stokes parameters for January 8, 9 and 11, where they say the measurements are significant. The values they report for q and u are of the same order as those we report here, but are not directly comparable. The equivalent width obtained from an LSD profile can be equated to a broad-band linear polarization measurement if one knows what scaling factor needs to be applied (Wade et al. 2000; Silvester et al. 2012). In Ap stars, this scaling factor is of the order of ∼3–10 and is always applied to increase the broad-band measurement to account for the fact that many regions of the band contain no significant spectral lines. In cooler dwarfs, with a greater number of spectral lines, we might expect it to be less. However, the relationship between the LSD amplitude (reported by Kochukhov et al. 2011) and the equivalent width is not readily predictable (Wade et al. 2000; Silvester et al. 2012), meaning that we cannot compare our results with Kochukhov et al. (2011)'s to determine a scaling factor.

The observations of ϵ Eri use similar sized telescopes with both instruments at the Cassegrain focus, which affords us the opportunity to compare the relative sensitivities of aperture and LSD techniques. Our total exposure time was 640 s, and we achieved a formal error of 5.3 ppm. Kochukhov et al. (2011)'s best precision is reported for January 8. On that night, their exposure time was 2000 s. Meaning that a roughly 8000 s exposure would be necessary to achieve the same precision as our broad-band aperture technique assuming photon-limited performance.

4.6.6 *Implications for exoplanet polarimetry*

The hot Jupiter system HD 189733 is the most promising target for the detection of scattered light from a planetary atmosphere. HD 189733b has been the subject of an ongoing controversy in the literature, a succinct run-down of which can be found in the recent work of Bott et al. (2016). In short, whilst observations by Berdyugina et al. (2008, 2011) report polarization levels of ∼100 ppm, where the largest signals are at the shortest wavelengths, these results have not been replicated by Wiktorowicz (2009) and Wiktorowicz et al. (2015), nor by Bott et al. (2016) who reports a possible polarization amplitude, matching the phase of the planet, of 29.4 ± 15.6 ppm (in a 500 nm short pass band that had an effective wavelength of 446.1 nm).

HD 189733 is a K1.5V ($B - V = 0.93$) BY Dra variable with starspot coverage ∼2 per cent, and from a determination we made from 96 observations in the PolarBase database (Petit et al. 2014), an extreme value of B_l of −17.3 ± 0.7 G. Calculations of the effect of starspots on HD 189733 based on their partial occulting of the stellar disc by Kostogryz et al. (2015) give only a 3 ppm variation. The possible effects of differential saturation modulated by stellar activity are mentioned by Bott et al. (2016) but appear not to have been considered by the other authors, and other stellar effects are usually assumed to be negligible. Our results presented here reveal linear polarization of tens of ppm for BY Dra variables with similar spectral types to HD 189733, which may be attributable to differential saturation associated with similarly strong magnetic fields. If differential saturation from starspots causes polarization in these stars, then it may also help explain the different results seen for HD 189733, given that stellar activity can be variable on time-scales of years. Although planet's orbital period (∼2.2 d; Triaud et al. 2010) and the stellar rotation period (∼11.8 d; Moutou et al. 2007) are quite different, the precision of the measurements at present, and the fact that Berdyugina et al. (2008, 2011) have not reported the exact timings of their measurements means that it is not possible to determine whether stellar activity has been mistaken for a planetary signal through signal aliasing.

The baseline polarization (i.e. that not tentatively attributed to the planet) determined by Bott et al. (2016) for HD 189733 was 70.1 ± 9.6 ppm, at a polarization angle of 20.°0 ± 3.9°, which they note is larger than is expected from interstellar polarization alone. Our model gives p_i as 20.0 ppm after a minor adjustment for the bluer effective wavelength. There are only three stars in the interstellar lList within 35° of HD 189733, and the closest one has quite a large uncertainty, and does not agree well with the other two; if we cautiously remove it, we make θ_i to be 14.°4. Subtracting the predicted interstellar polarization from the baseline gives $\hat{p} = 52.6 \pm 9.6$ ppm as the likely contribution from stellar activity. This is similar to, but a little higher than determined for ξ Boo that is a warmer star but has a similar $|B_l|_{max}$ value. So, the determination is consistent with differential saturation producing higher polarization at bluer wavelengths and/or in cooler stars with similar activity levels.

The nature of stellar activity may be similarly important for observations of τ Boo. A signal from τ Boo b was unsuccessfully sought by Lucas et al. (2009), who, however, noted that greater scatter in their results correlated with starspot activity. In that system, a large hotspot has been observed leading the subplanetary point by 60°–70°, and starspots have also been seen to move in phase with the planet (Lanza 2008). τ Boo is a warmer star ($B - V = 0.49$) than those we recorded significant polarizations for here, and its extreme value of B_l from 177 observations from BCool and PolarBase is +4.6 ± 0.4 G. These facts combined suggest that the contribution of magnetic activity is likely to be smaller than for HD 189733.

Because the rotation period of HD 189733 is different from the orbital period of HD 189733b, a starspot signal could be removed. Performing a similar task may be more difficult for τ Boo b but with better characterization of polarization due to differential saturation it should be possible. Saar & Huovelin (1993) and Stift (1997)'s models predict signals from differential saturation that are highly wavelength-dependant and do not vary smoothly. In contrast, the polarization due to Rayleigh scattering from exoplanetary clouds can be expected to be a fairly smooth function of wavelength that rises to the blue (Evans et al. 2013). Therefore, simultaneous observations in multiple pass bands could be used to decouple the two effects.

5 CONCLUSIONS

We have made a short linear polarimetric survey of nearby FGK dwarfs at ppm precision. Amongst the sample were debris disc host stars and active stars. Our initial statistical analysis showed active stars to be more polarized than ordinary FGK dwarfs, but no discernable difference between inactive debris disc stars and other inactive stars.

We added our data on ordinary FGK dwarfs to literature measurements of other nearby stars, which improved our knowledge of the local ISM. The data show some alignment with the local ISM field, but we do not see the same Loop I Superbubble structure associated with the region at 50–100 pc. We find that there are broadly two regions with differing polarization with distance relations within

100 pc. Although the ISM is patchy, above $b = +30$, we make the relationship to be

$$p_i = (0.261 \pm 0.017)d, \quad (7)$$

where p_i is in ppm and d is in parsecs. For the stars below $b = +30$ and within 14.5 pc, we find

$$p_i = (0.800 \pm 0.120)d, \quad (8)$$

below $b = +30$, and beyond 14.5 pc, the relationship is

$$p_i = (1.644 \pm 0.298)(d - 14.5) + (11.6 \pm 1.7). \quad (9)$$

We also determined that the position angles of stars polarized by the ISM are increasingly well aligned for separations decreasing from 35°.

We used the information obtained on the ISM to construct a simple model for determining interstellar polarization. Up until now, subtractions of interstellar polarization within the LHB have required additional measurements of control stars. Our model will become increasingly powerful as more measurements of nearby stars are added at ppm precisions, potentially eliminating the need for control measurements. This development will drastically reduce the time required for precision polarimetric work on nearby objects.

After subtracting interstellar polarization using our model, we find the mean polarization of the active stars to be 23.0 ± 2.2 ppm compared to 2.9 ± 1.9 ppm for the inactive non-debris disc stars. The most polarized star in our survey was the active star ξ Boo at 44.3 ± 5.2 ppm. Both these figures are much less than reported by other researchers. Although the data may be explained by polarization either through Rayleigh scattering from large (∼18 per cent) starspots at close to optimal alignments, or differential saturation from localized regions of strong magnetic fields-like starspots with filling factors greater than ∼0.25–2.0 per cent, we suggest differential saturation attributable to weaker global scale magnetic fields to be the most likely mechanism. The most polarized active stars also have large net longitudinal magnetic fields. The result has important implications for efforts to detect scattered polarized light from hot Jupiter clouds in the combined light of star and planet. Positive detections for planets orbiting active stars will be more challenging than previously assumed. An improved understanding of intrinsic polarization in active stars will help overcome the challenges.

For debris disc host stars, we find a mean of 7.8 ± 2.9 ppm after interstellar subtraction, with a marginal 3σ detection for the disc around HD 207129 that amounts to a polarization ∼30 per cent of its infrared excess. Upon examining our data conscientiously system by system, we can explain the signals in most systems by the disc infrared excess and geometry with respect to the aperture. A high p: $(L_{\rm dust}/L_\star)$ ratio for ζ^2 Ret corroborates literature reports that its disc is asymmetric.

ACKNOWLEDGEMENTS

This work was supported by the Australian Research Council through Discovery Project grant DP160103231. JPM is supported by a UNSW VC's Postdoctoral Research Fellowship. The authors thank the Director and staff of the Australian Astronomical Observatory for their advice and support with interfacing HIPPI to the AAT and during our observing runs on the telescope. We thank Daniela Optiz and Gesa Gruening for their assistance in making observations in 2016 February/March and 2016 June, respectively. We acknowledge the use of the SIMBAD database and this research has made use of the VizieR Service at Centre de Données Astronomiques de Strasbourg. We wish to thank the anonymous referee for valuable feedback that has improved this paper.

REFERENCES

Absil O. et al., 2013, A&A, 555, A104
Akeson R. L. et al., 2013, PASP, 125, 989
Alekseev I. Y., 2003, Astron. Rep., 47, 430
Atri D., 2016, MNRAS, 463, L64
Babcock H. W., 1949, ApJ, 110, 126
Backman D. et al., 2009, ApJ, 690, 1522
Bagnulo S., Landi Degl'Innocenti E., Landolfi M., Leroy J. L., 1995, A&A, 295, 459
Bailey J., Lucas P. W., Hough J. H., 2010, MNRAS, 405, 2570
Bailey J., Kedziora-Chudczer L., Cotton D. V., Bott K., Hough J. H., Lucas P. W., 2015, MNRAS, 449, 3064
Bailey J., Cotton D. V., Kedziora-Chudczer L., 2017, MNRAS, 465, 1601
Behr A., 1959, PhD thesis, Univ. Gottingen
Berdyugina S. V., Berdyugin A. V., Fluri D. M., Piirola V., 2008, ApJ, 673, L83
Berdyugina S. V., Berdyugin A. V., Fluri D. M., Piirola V., 2011, ApJ, 728, L6
Bott K., Bailey J., Kedziora-Chudczer L., Cotton D. V., Lucas P. W., Marshall J. P., Hough J. H., 2016, MNRAS, 459, L109
Chavez-Dagostino M. et al., 2016, MNRAS, 462, 2285
Clarke D., 1991, Vistas Astron., 34, 303
Clarke D., 2010, Stellar Polarimetry. Wiley-VCH Verlag GmbH & Co. KGaA, Weinheim
Cotton D. V., Bailey J., Kedziora-Chudczer L., Bott K., Lucas P. W., Hough J. H., Marshall J. P., 2016a, MNRAS, 455, 1607
Cotton D. V., Bailey J., Kedziora-Chudczer L., Bott K., Lucas P. W., Hough J. H., Marshall J. P., 2016b, MNRAS, 460, 18
Cotton D. V., Marshall J. P., Bott K., Kedziora-Chudczer L., Bailey J., 2016c, in Short W., Caprarelli G., eds, Proc. 15th Aust. Space Res. Conf. (ASRC15), National Space Society of Australia (NSSA), Australia, p. 55
Cuntz M., Saar S. H., Musielak Z. E., 2000, ApJ, 533, L151
de Geus E. J., 1992, A&A, 262, 258
Defrère D. et al., 2015, ApJ, 799, 42
di Folco E. et al., 2007, A&A, 475, 243
Donati J.-F., Landstreet J. D., 2009, ARA&A, 47, 333
Donati J.-F., Semel M., Carter B. D., Rees D. E., Collier Cameron A., 1997, MNRAS, 291, 658
Duchêne G. et al., 2014, ApJ, 784, 148
Duquennoy A., Mayor M., 1991, A&A, 248, 485
Dyck H. M., Jennings M. C., 1971, AJ, 76, 431
Eiroa C. et al., 2010, A&A, 518, L131
Eiroa C. et al., 2013, A&A, 555, A11
Elias N. M., II, Dorren J. D., 1990, Inf. Bull. Var. Stars, 3541
Ertel S. et al., 2014, A&A, 570, A128
Ertel S. et al., 2016, A&A, 595, A44
Evans T. M. et al., 2013, ApJ, 772, L16
Faramaz V. et al., 2014, A&A, 563, A72
Fares R. et al., 2010, MNRAS, 406, 409
Frisch P. C., 1990, in Grzedzielski S., Page D. E., eds, Physics of the Outer Heliosphere. Pergamom Press, Oxford, p. 19
Frisch P. C., 1995, Space Sci. Rev., 72, 499
Frisch P. C., 1996, Space Sci. Rev., 78, 213
Frisch P. C., Schwadron N. A., 2014, ASPC, 484, 42
Frisch P. C. et al., 2010, ApJ, 724, 1473
Frisch P. C. et al., 2016, J. Phys. Conf. Ser., 767, 012010
Frisch P. C., Redfield S., Slavin J. D., 2011, ARA&A, 49, 237
Frisch P. C. et al., 2012, ApJ, 760, 106
Frisch P. C. et al., 2015, ApJ, 814, 112
Giuricin G., Mardirossian F., Mezzetti M., 1984, ApJS, 54, 421
Glebocki R., Musielak G., Stawikowski A., 1980, AcA, 30, 453
Graham J. R., Kalas P. G., Matthews B. C., 2007, ApJ, 654, 595

Greaves J. S. et al., 2014, ApJ, 791, L11
Hengst S., Marshall J. P., Horner J., Marsden S., 2017, MNRAS, in press
Heiles C., 1996, in Roberge W. G., Whittet D. C. B., eds, ASP Conf. Ser. Vol. 97, Polarimetry of the Interstellar Medium. Astron. Soc. Pac., San Francisco, p. 457
Heiles C., 1998, ApJ, 498, 689
Heiles C., 2009, in Smith R. K., Snowden S. L., Kuntz K. D., eds, AIP Conf. Ser. Vol. 1156, The Local Bubble and Beyond II. Am. Inst. Phys., New York, p. 199
Helled R. et al., 2014, in Beuther H., Klessen R. S., Dullemond C. P., Henning T., eds, Protostars and Planets VI. Univ. Arizona Press, Tucson, AZ, p. 643
Hempelmann A., Mittag M., Gonzalez-Perez J. N., Schmitt J. H. M. M., Schröder K. P., Rauw G., 2016, A&A, 586, A14
Hough J. H., Lucas P. W., Bailey J. A., Tamura M., Hirst E., Harrison D., Bartholomew-Biggs M., 2006, PASP, 118, 1302
Huber D. et al., 2011, ApJ, 731, 94
Huovelin J., Saar S. H., 1991, ApJ, 374, 319
Huovelin J., Saar S. H., Tuominen I., 1988, ApJ, 329, 882
Jackson R. J., Jeffries R. D., 2013, MNRAS, 431, 1883
Jeffers S. V., Petit P., Marsden S. C., Morin J., Donati J.-F., Folsom C. P., 2014, A&A, 569, A79
Jenkins J. S. et al., 2006, MNRAS, 372, 163
Kemp J. C., Henson G. D., Barbour M. S., Kraus D. J., Collins G. W., II, 1983, ApJ, 273, L85
Kemp J. C., Henson G. D., Kraus D. J., Beardsley I. S., Carroll L. C., Duncan D. K., 1986, ApJ, 301, L35
Kemp J. C., Henson G. D., Kraus D. J., Dunaway M. H., 1987a, BAAS, 19, Q752
Kemp J. C., Karitskaya E. A., Kumsiashvili M. I., Lyutij V. M., Kruzina T. S., Cherepashchuk A. M., 1987b, Astron. Zh., 64, 326
Kennedy G. M. et al., 2015, MNRAS, 449, 3121
Kochukhov O. et al., 2011, ApJ, 732, L19
Kostogryz N. M., Berdyugina S. V., 2015, A&A, 575, A89
Kostogryz N. M., Berdyugina S. V., Yakobchuk T. M., 2015, in van Belle G. T., Harris H. C., eds, Proc. Conf. 18th Cambridge Workshop on Cool Stars, Stellar Systems, and the Sun. p. 773
Krist J. E. et al., 2010, AJ, 140, 1051
Lagrange A.-M., Desort M., Galland F., Udry S., Mayor M., 2009, A&A, 495, 335
Lallement R., Welsh B. Y., Vergely J. L., Crifo F., Sfeir D., 2003, A&A, 411, 447
Landi Degl'Innocenti E., 1982, A&A, 110, 25
Lanza A. F., 2008, A&A, 487, 1163
Lawler S. M. et al., 2014, MNRAS, 444, 2665
Leroy J. L., 1989, A&A, 215, 360
Leroy J. L., 1990, A&A, 237, 237
Leroy J. L., 1993, A&A, 274, 203
Löhne T. et al., 2012, A&A, 537, A110
Lucas P. W., Hough J. H., Bailey J. A., Tamura M., Hirst E., Harrison D., 2009, MNRAS, 393, 229
McCaughrean M. J., Close L. M., Scholz R.-D., Lenzen R., Biller B., Brandner W., Hartung M., Lodieu N., 2004, A&A, 413, 1029
McLean I. S., 1980, in Plavec M. J., Popper D. M., Ulrich R. K., eds, Proc. IAU Symp. 88, Close Binary Stars: Observations and Interpretation. Kluwer, Dodrecht, p. 65
Marsden S. C. et al., 2014, MNRAS, 444, 3517
Marshall J. P. et al., 2011, A&A, 529, A117
Marshall J. P. et al., 2014, A&A, 565, A15
Marshall J. P. et al., 2016, ApJ, 825, 124
Martínez-Arnáiz R., Maldonado J., Montes D., Eiroa C., Montesinos B., 2010, A&A, 520, A79
Middelkoop F., 1982, A&A, 107, 31
Montesinos B. et al., 2016, A&A, 593, A51
Morgenthaler A. et al., 2012, A&A, 540, A138
Moro-Martín A. et al., 2015, ApJ, 801, 143
Moutou C. et al., 2007, A&A, 473, 651
Naghizadeh-Khouei J., Clarke D., 1993, A&A, 274, 968
Noyes R. W., Weiss N. O., Vaughan A. H., 1984, ApJ, 287, 769
Patel M. K., Pandey J. C., Karmakar S., Srivastava D. C., Savanov I. S., 2016, MNRAS, 457, 3178
Pecaut M. J., Mamajek E. E., 2013, ApJS, 208, 9
Perryman M. A. C. et al., 1997, A&A, 323, L49
Petit P., Louge T., Théado S., Paletou F., Manset N., Morin J., Marsden S. C., Jeffers S. V., 2014, PASP, 126, 469
Piskunov N. et al., 2011, The Messenger, 143, 7
Redfield S., Linsky J. L., 2008, ApJ, 673, 283
Reiners A., Schmitt J. H. M. M., Kürster M., 2001, A&A, 376, L13
Rieke G. H., Gáspár A., Ballering N. P., 2016, ApJ, 816, 50
Rosén L., Kochukhov O., Wade G. A., 2013, MNRAS, 436, L10
Rosén L., Kochukhov O., Wade G. A., 2015, ApJ, 805, 169
Saar S. H., Huovelin J., 1993, ApJ, 404, 739
Salter C. J., 1983, Bull. Astron. Soc. India, 11, 1
Santos F. P., Corradi W., Reis W., 2011, ApJ, 728, 104
Schaaf F., 2008, The Brightest Stars: Discovering the Universe through the Sky's Most Brilliant Stars. John Wiley & Sons, Inc., Hoboken
Schröder C., Reiners A., Schmitt J. H. M. M., 2009, A&A, 493, 1099
Schüppler C. et al., 2015, A&A, 581, A97
Seager S., Whitney B. A., Sasselov D. D., 2000, ApJ, 540, 504
Serkowski K., 1962, Adv. Astron. Astrophys., 1
Sierchio J. M., Rieke G. H., Su K. Y. L., Gáspár A., 2014, ApJ, 785, 33
Silvester J., Wade G. A., Kochukhov O., Bagnulo S., Folsom C. P., Hanes D., 2012, MNRAS, 426, 1003
Snik F. et al., 2011, in Kuhn J. R., Harrington D. M., Lin H., Berdyugina S. V., Trujillo-Bueno J., Keil S. L., Rimmele T., eds, ASP Conf. Ser. Vol. 437, Solar Polarization 6. Astron. Soc. Pac., San Francisco, p. 237
Soubiran C., Le Campion J.-F., Brouillet N., Chemin L., 2016, A&A, 591, A118
Stephens I. W., Looney L. W., Dowell C. D., Vaillancourt J. E., Tassis K., 2011, ApJ, 728, 99
Stift M. J., 1997, in Schmieder B., del Toro Iniesta J. C., Vazquez M., eds, ASP Conf. Ser. Vol. 118, 1st Advances in Solar Physics Euroconference. Astron. Soc. Pac., San Francisco, p. 242
Su K. Y. L. et al., 2013, ApJ, 763, 118
Tilley D. A., Balsara D. S., Howk J. C., 2006, MNRAS, 371, 1106
Tinbergen J., 1982, A&A, 105, 53
Tinbergen J., Zwaan C., 1981, A&A, 101, 223
Toner C. G., Gray D. F., 1988, ApJ, 334, 1008
Triaud A. H. M. J. et al., 2010, A&A, 524, A25
Trilling D. E. et al., 2008, ApJ, 674, 1086
Wade G. A., Donati J.-F., Landstreet J. D., Shorlin S. L. S., 2000, MNRAS, 313, 851
Wiktorowicz S. J., 2009, ApJ, 696, 1116
Wiktorowicz S. J., Matthews K., 2008, PASP, 120, 1282
Wiktorowicz S. J., Nofi L. A., Jontof-Hutter D., Kopparla P., Laughlin G. P., Hermis N., Yung Y. L., Swain M. R., 2015, ApJ, 813, 48
Wittenmyer R. A. et al., 2014, ApJ, 783, 103
Wyatt M. C. et al., 2012, MNRAS, 424, 1206
Zechmeister M. et al., 2013, A&A, 552, A78

APPENDIX A: STARS REPRESENTATIVE OF INTERSTELLAR POLARIZATION

Table A1 lists 58 stars observed with either HIPPI or PlanetPol, which are believed to have polarization characteristic of the ISM. The 14 inactive non-debris disc FGK dwarfs and e Eri and η Crv observations reported here are used in conjunction with these tabulated observations to define interstellar polarization in this paper. In the table, all objects cited as Bailey et al. (2010) have been converted to g' by multiplication of the magnitude of polarization by 1.2; see Marshall et al. (2016). Slight differences between the other results tabulated here and the original reference are attributable to minor improvements made in the post-observation analysis pipeline since publication. Polarization angle errors quoted here are derived

Table A1. Additional literature stars for the interstellar list.

HD	Sp. type	RA (hh mm ss)	Dec. (dd mm ss)	Galactic l (°)	b (°)	d (pc)	p^a (ppm)	θ (°)	θ_G (°)	Ref	Notes[b]
739	F5V	00 11 44.0	−35 07 59	347.18	−78.34	21.3	39.3 ± 11.4	71.0 ± 8.6	120.2	Marshall et al. (2016)	
2151	G0V	00 25 39.2	−77 15 18	304.78	−39.78	7.5	5.8 ± 1.4	95.4 ± 7.2	102.6	Updated.	L
2261	K0.5IIIb	00 26 16.9	−42 18 18	320.00	−73.97	23.7	18.9 ± 5.5	62.3 ± 8.6	82.8	Cotton et al. (2016b)	
4128	K0III	00 43 35.2	−17 59 12	111.34	−80.68	29.4	23.5 ± 6.6	95.1 ± 8.3	106.0	Cotton et al. (2016a)	
4308	G8V	00 44 39.0	−65 38 52	304.06	−51.46	21.9	24.6 ± 15.5	120.4 ± 22.5	122.7	Marshall et al. (2016)	
7693	K2V+K3V	01 15 01.0	−68 49 08	299.75	−48.16	21.6	162.8 ± 22.7	96.8 ± 4.0	88.8	Marshall et al. (2016)	i
12311	F0IV	01 58 45.9	−61 34 12	289.45	−53.76	21.9	42.4 ± 7.2	159.2 ± 4.9	133.3	Marshall et al. (2016)	
18622J	A4III	02 58 15.7	−40 18 17	247.84	−60.73	49.5	74.0 ± 7.1	31.5 ± 2.8	138.7	Cotton et al. (2016a)	
28556	F0IV	04 30 37.4	13 43 28	182.50	−22.97	45.2	50.8 ± 26.1	7.1 ± 18.0	135.2	Marshall et al. (2016)	ii
45348	A9II	06 23 57.1	−52 41 45	261.22	−25.29	95.9	113.0 ± 1.2	116.2 ± 0.3	38.7	Bailey et al. (2015)	v
48915	A0V	06 45 09.2	−16 42 47	227.23	−8.89	2.6	1.8 ± 0.6	163.3 ± 11.4	99.3	Updated	L
74956	A1Va(n)	08 44 42.2	−54 42 32	272.08	−7.37	24.7	44.5 ± 6.8	127.9 ± 4.4	75.7	Cotton et al. (2016a)	
80007	A1III	09 13 12.0	−69 43 02	285.98	−14.41	34.7	23.9 ± 2.6	74.4 ± 3.1	25.8	Cotton et al. (2016a)	
81797	K3II-III	09 27 35.2	−08 39 31	241.49	29.05	55.3	8.8 ± 3.7	170.8 ± 13.7	118.7	Cotton et al. (2016a)	iii, v
89025	F0IIIa	10 16 41.4	23 25 01	210.22	54.95	84.0	16.9 ± 2.9	107.3 ± 5.0	32.2	Bailey et al. (2010)	v
93497	G6III	10 46 46.1	−49 25 12	283.03	8.57	35.5	33.5 ± 4.3	123.4 ± 3.7	95.6	Cotton et al. (2016a)	
95689	G9III+A7V	11 03 43.7	61 45 04	142.85	51.01	37.7	11.2 ± 1.1	141.5 ± 2.8	101.9	Bailey et al. (2010)	
96833	K1III	11 09 39.8	44 29 55	165.80	63.23	44.3	4.6 ± 2.5	109.3 ± 19.3	51.6	Bailey et al. (2010)	
97603	A5IV(n)	11 14 06.5	20 31 25	224.24	66.83	17.9	4.4 ± 2.8	158.6 ± 22.7	90.2	Bailey et al. (2010)	
97633	A2IV	11 14 14.4	15 25 47	235.37	64.59	50.6	8.3 ± 3.2	25.2 ± 12.6	146.8	Bailey et al. (2010)	v
102224	K0.5IIIb	11 46 03.0	47 46 46	150.32	65.72	56.3	12.1 ± 3.1	148.9 ± 7.6	111.6	Bailey et al. (2010)	v
102509	A7V	11 48 59.1	20 13 08	235.01	73.94	71.3	14.0 ± 4.4	100.5 ± 9.4	39.2	Bailey et al. (2010)	v
108767	A0IV	12 29 51.9	−16 30 57	295.48	46.04	26.6	18.7 ± 3.8	70.0 ± 5.8	63.0	Cotton et al. (2016a)	
109379	G5II	12 34 24.0	−23 23 48	297.88	39.30	42.8	34.5 ± 3.8	76.1 ± 3.2	71.1	Cotton et al. (2016a)	
110304	A1IV+A0IV	12 41 31.0	−48 57 36	301.26	13.88	39.9	61.6 ± 4.2	63.8 ± 1.9	61.4	Cotton et al. (2016a)	
110379J	F0IV+F0IV	12 41 39.6	−01 26 58	297.84	61.33	11.7	7.6 ± 4.0	112.5 ± 18.6	107.9	Cotton et al. (2016a)	
113226	G8III	13 02 10.6	10 57 33	312.31	73.64	33.6	6.8 ± 1.2	3.1 ± 5.1	11.5	Bailey et al. (2010)	
115659	G8III	13 18 55.2	−23 10 17	311.10	39.27	40.5	5.6 ± 4.2	36.4 ± 26.2	44.2	Cotton et al. (2016a)	
116656	A1.5Vas	13 23 55.5	54 55 31	113.11	61.57	26.3	9.1 ± 1.9	173.2 ± 5.9	8.6	Bailey et al. (2010)	
121370	G0IV	13 54 41.1	18 23 52	5.29	73.03	11.4	4.2 ± 2.0	167.4 ± 16.0	43.3	Bailey et al. (2010)	
123129	K0III	14 06 40.9	−36 22 12	319.45	24.08	18.0	42.6 ± 3.3	56.7 ± 2.2	74.9	Cotton et al. (2016a)	
124897	K0III	14 15 39.7	19 10 57	15.05	69.11	11.3	7.5 ± 1.8	30.7 ± 7.0	94.1	Bailey et al. (2010)	iv
127665	K3III	14 31 49.8	30 22 17	47.29	67.80	49.1	12.3 ± 2.8	124.5 ± 6.7	30.2	Bailey et al. (2010)	
127762	A7IV(n)	14 32 04.7	38 18 30	67.27	66.17	26.6	4.3 ± 1.9	109.1 ± 15.2	178.3	Bailey et al. (2010)	
130841	A3V	14 50 52.8	−16 02 30	340.33	38.01	23.2	27.8 ± 3.4	142.1 ± 3.4	176.2	Cotton et al. (2016a)	v
140573	K2IIIb	15 44 16.1	06 25 32	14.21	44.08	22.7	4.4 ± 1.7	16.3 ± 12.3	74.1	Updated	L
147547	A9IIIbn	16 21 55.2	19 09 11	35.25	41.30	59.1	15.9 ± 3.2	47.8 ± 5.9	117.7	Bailey et al. (2010)	v
148856	G7IIIa Fe	16 30 13.2	21 29 23	39.01	40.21	42.7	22.5 ± 1.6	24.5 ± 2.1	96.1	Bailey et al. (2010)	
150680	G0IV	16 41 17.2	31 36 10	52.66	40.29	10.7	11.5 ± 3.1	51.7 ± 8.0	130.7	Bailey et al. (2010)	
151680	K1III	16 50 10.2	−34 17 33	348.81	6.56	20.1	28.9 ± 6.7	34.4 ± 6.8	84.8	Cotton et al. (2016a)	
153210	K2III	16 57 40.1	09 22 30	28.37	29.50	28.0	14.4 ± 1.9	64.1 ± 3.8	127.9	Bailey et al. (2010)	
153808	A0V	17 00 17.4	30 55 35	52.86	36.18	47.5	14.9 ± 4.7	66.0 ± 9.5	142.8	Bailey et al. (2010)	
155125	A2IV-V	17 10 22.7	−15 43 30	6.71	14.01	25.8	57.2 ± 3.6	147.7 ± 1.8	23.5	Cotton et al. (2016a)	
156164	A1IVn+G4IV-V	17 15 01.9	24 50 21	46.83	31.42	23.0	9.4 ± 2.9	66.2 ± 9.1	138.0	Bailey et al. (2010)	
159532	F1III	17 37 19.1	−43 59 52	347.14	−5.98	83.4	154.4 ± 2.9	94.0 ± 0.6	151.7	Cotton et al. (2016a)	v
159561	A5III	17 34 56.1	12 33 36	35.89	22.57	14.9	28.1 ± 2.4	30.8 ± 2.4	96.1	Bailey et al. (2010)	
161096	K2III	17 43 28.4	04 34 02	29.22	17.19	25.1	38.6 ± 2.6	27.9 ± 1.9	90.6	Bailey et al. (2010)	
161797	G5IV	17 46 27.5	27 43 14	52.44	25.63	8.3	11.1 ± 2.5	21.0 ± 6.4	92.0	Bailey et al. (2010)	
163588	K2III	17 53 31.7	56 52 22	85.16	30.23	34.5	4.5 ± 3.7	51.1 ± 28.1	136.3	Bailey et al. (2010)	
163993	G8III	17 57 45.9	29 14 52	54.91	23.77	41.9	29.2 ± 2.9	10.1 ± 2.8	80.8	Bailey et al. (2010)	
164058	K5III	17 56 36.4	51 29 20	79.06	29.22	47.3	87.9 ± 1.4	145.0 ± 0.5	46.7	Bailey et al. (2010)	
165135	K1III	18 05 48.5	−30 25 25	0.92	−4.53	29.5	38.5 ± 16.1	173.8 ± 13.8	54.5	Cotton et al. (2016a)	
168775	K2III	18 19 51.7	36 03 52	63.52	21.54	77.2	127.8 ± 3.2	6.1 ± 0.7	77.2	Bailey et al. (2010)	v
169916	K0IV	18 27 58.3	−25 25 16	7.66	−6.52	20.7	54.2 ± 8.2	140.1 ± 4.5	22.8	Cotton et al. (2016a)	
176687	A2.5Va+A4IV	19 02 36.7	−29 52 48	6.84	−15.35	27.3	28.2 ± 3.6	135.9 ± 3.7	22.7	Marshall et al. (2016)	
187691	F8V	19 51 01.6	10 25 57	49.14	−8.20	19.2	18.9 ± 9.7	119.3 ± 17.8	179.4	Marshall et al. (2016)	
188119	G8III+F5III	19 48 10.4	70 16 17	102.43	20.83	45.4	1.8 ± 3.1	63.4 ± 40.2	130.9	Bailey et al. (2010)	iii
207098	A7III	21 47 02.3	−16 07 48	37.60	−46.01	11.8	29.6 ± 16.2	137.3 ± 19.4	24.4	Cotton et al. (2016a)	

Notes. [a] g'-band equivalent.
[b] L indicates a low polarization standard. For numeric notes, see the text of Appendix A.

in the same way as those in the main body of the paper, regardless of how they were reported in the original reference. Low polarization standards where the updated measurements reported correspond to the aggregate measurements of a number of observing runs.

Some stars have been excluded from some or all parts of the interstellar determinations made in the paper as follows.

(i) HD 7693 is excluded from Section 4.2.1 as an outlier in polarization magnitude, but included in determining the angle interstellar

polarization in later sections – the angle determined for its primary HD 7788 is very similar; see Marshall et al. (2016).

(ii) HD 28556 is excluded from determinations of interstellar polarization magnitude and angle due to the size of the error, and the relatively few stars at that distance.

(iii) α Hya and ϵ Dra are included in the p/d determination for the $b > +30$ group rather than the $b < +30$ group.

(iv) Arcturus exhibits variable polarization in the *B* band according to Kemp et al. (1983), the measurement utilized here corresponds to the red (575–1025 nm) bandpass of PlanetPol.

(v) α^2 Lib is excluded from analysis on account of a discrepant magnitude and angle of polarization relative to neighbouring stars in a region where both are well defined.

(vi) Stars at greater than 50 pc are not used in Sections 4.2.3 and 4.3.

This paper has been typeset from a TEX/LATEX file prepared by the author.